

Gas Accretion onto the Milky Way

Philipp Richter

Abstract The Milky Way is surrounded by large amounts of gaseous matter that are slowly being accreted over cosmic timescales to support star formation in the disk. The corresponding gas-accretion rate represents a key parameter for the past, present, and future evolution of the Milky Way. In this chapter, we discuss our current understanding of gas accretion processes in the Galaxy by reviewing past and recent observational and theoretical studies. The first part of this review deals with the spatial distribution of the different gas phases in the Milky Way halo, the origin of the gas, and its total mass. The second part discusses the gas dynamics and the physical processes that regulate the gas flow from the outer Galactic halo to the disk. From the most recent studies follows that the present-day gas accretion rate of the Milky Way is a few solar masses per year, which is sufficient to maintain the Galaxy's star-formation rate at its current level.

1 Introduction

We start this chapter on Galactic accretion with an introduction, in which we first summarize early measurements of circumgalactic gas and the star-formation history of the Milky Way from a historical perspective. We then shortly discuss the role of gas accretion processes in Milky-Way type galaxies in a cosmological context and highlight their importance for galaxy evolution in general. The introduction section ends with a proper definition of the gas-accretion rate, dM_{gas}/dt , and an assessment of the physical parameters that need to be constrained from observations and simulations to estimate dM_{gas}/dt for the Milky Way.

Philipp Richter
Institut für Physik und Astronomie, Universität Potsdam, Karl-Liebknecht-Str. 24/25, 14476 Golm,
Germany e-mail: prichter@astro.physik.uni-potsdam.de

1.1 Historical remarks

The presence of gas above/below the Milky Way disk has been established already more than 60 years ago, when absorption-line measurements demonstrated the presence of gas clouds at high galactic latitudes that exhibit relatively high radial velocities (Adams 1949; Münch 1952; Münch & Zirin 1961). In 1956, Lyman Spitzer argued that these structures, if located in the halo, must be surrounded by a hot, gaseous medium (he named this medium the *Galactic Corona*) that provides the necessary pressure-confinement of these clouds, otherwise they should disperse on relatively short timescales (Spitzer 1956).

With the new receiver technologies and the resulting improved sensitivity of radio telescopes in the 1960s, high-velocity HI 21 cm emission at high galactic latitudes was found by Muller et al. (1963), Smith (1963), Dieter (1964), Blaauw & Tolbert (1966), Hulsbosch & Raimond (1966), and Mathewson (1967), supporting the conclusions from the earlier absorption-line measurements. The observed distribution of radial velocities of the 21 cm emission features lead to the definition of two classes of Galactic halo clouds: as “high-velocity clouds” (HVCs) those halo structures were labeled that have radial velocities, $|\nu_{\text{LSR}}| > 100 \text{ km s}^{-1}$, while features with somewhat smaller radial velocities ($|\nu_{\text{LSR}}| \approx 30 - 100 \text{ km s}^{-1}$) were given the name “intermediate-velocity clouds” (IVCs). As will be discussed later, there also might exist a population of halo clouds with very low LSR velocities (“low-velocity clouds” (LVCs), similar to those in the disk.

Several scenarios for the origin of the 21 cm neutral halo clouds were discussed by Jan Oort in 1966, among which the infall of intergalactic gas, the accretion of gas from satellite galaxies, the condensation of neutral gas patches from cooling coronal gas, and the ejection of gaseous material from the Milky Way disk were regarded as plausible scenarios (Oort 1966). Indeed, as we will discuss in this review, these scenarios are still up-to-date.

The need for feeding the Milky Way disk with low-metallicity gas also comes from early studies of the Galaxy’s star-formation activity and stellar content. Already in the 1970s it was realized that star-formation in the Milky Way would have come to a halt early on, if the Galaxy was not fed with fresh material from outside. This is because the gas-consumption time scale (even for a moderate star-formation rate of $\sim 1 M_{\odot} \text{ yr}^{-1}$) is short compared to the age of the Milky Way (Larson 1972). Another argument for gas accretion comes from the observed metallicity distribution of low-mass stars in the solar neighborhood, which cannot be reproduced by closed-box models of the chemical evolution of the stellar disk. To match the observations, such models *require* the continuous accretion of metal-poor gas (van den Bergh 1962; Chiappini et al. 2001). These findings provide additional strong arguments that the Milky Way has accreted (and is still doing so) large amounts of low-metallicity gas to continuously built up its stellar content as observed today.

In conclusion, the observed presence of large amounts of gas above/below the disk, the past and present star-formation rate of the Milky Way, and the metallicity distribution of low-mass stars in the solar neighborhood demonstrate that gas

accretion represents an important process that has strong implications for the past, present, and future evolution of our Galaxy.

1.2 Cosmological context

In the overall context of galaxy formation in the Universe, gas accretion and feedback nowadays are regarded as the main processes that regulate the star-formation activity in galaxies. Many of the cosmological aspects of gas accretion in galaxies will be discussed in detail in other chapters of this book. Still, for our discussion on gas accretion in the Milky Way, the main aspects need to be summarized here.

In the conventional sketch of galaxy formation, gas is falling into a dark matter (DM) halo and then is shock-heated to approximately the halo virial temperature (a few 10^6 K, typically), residing in quasi-hydrostatic equilibrium with the DM potential well (Rees & Ostriker 1977). The gas then cools and sinks into the center of the potential where it is transformed into stars. This model is often referred to as the ‘hot mode’ of gas accretion. It has been argued that for smaller DM potential wells the infalling gas may reach the disk *directly* at much shorter timescales, without being shock-heated to the virial temperature (‘cold mode’ of gas accretion; e.g., White & Rees 1978; Kereš et al. 2005). In the latter case, the star-formation rate of the central galaxy would be directly coupled to its gas-accretion rate (White & Frenk 1991). In these simple pictures, the dominating gas-accretion mode depends on the mass and the redshift of the galaxy (e.g., Birnboim & Dekel 2003; Kereš et al. 2005), where at low redshift the critical halo mass that separates the hot mode from the cold mode is $\sim 10^{12} M_{\odot}$ (van de Voort et al. 2011). However, the underlying physics that describes the large-scale flows of multi-phase gas from the outer to the inner regions of a dynamically evolving galaxy is highly complicated (e.g. Mo & Miralda-Escude 1996; Maller & Bullock 2004). To understand these processes, high-resolution hydrodynamical simulations with well-defined initial conditions (e.g. Bauermeister et al. 2010; Fumagalli et al. 2011; van de Voort & Schaye 2012; Vogelsberger et al. 2012; Shen et al. 2013) are required. Therefore, even the most advanced hydrodynamical simulations do not provide tight constraints for the gas-accretion rate of *individual* galaxies without knowing their exact halo masses, their cosmological environment, and the initial circumgalactic gas distribution (Nuza et al. 2014; hereafter referred to as N14).

Next to the feeding of the halos of Milky-Way type galaxies through intergalactic gas, galactic-fountain type processes (from supernova (SN) feedback; Fraternali & Binney 2008) and mergers with satellite galaxies (Di Teodoro & Fraternali 2014) need to be considered. The vast amounts of neutral and ionized gas carried by the Magellanic Stream underline the importance of merger processes for the Milky Way’s gas-accretion rate (D’Onghia & Fox 2016; see Sect. 2). The preconditions under which such gas clouds are generated and falling toward the disk are different from those for clouds being accreted from the intergalactic medium (IGM; e.g., Peek 2009) and thus they need to be explored separately by both observations and

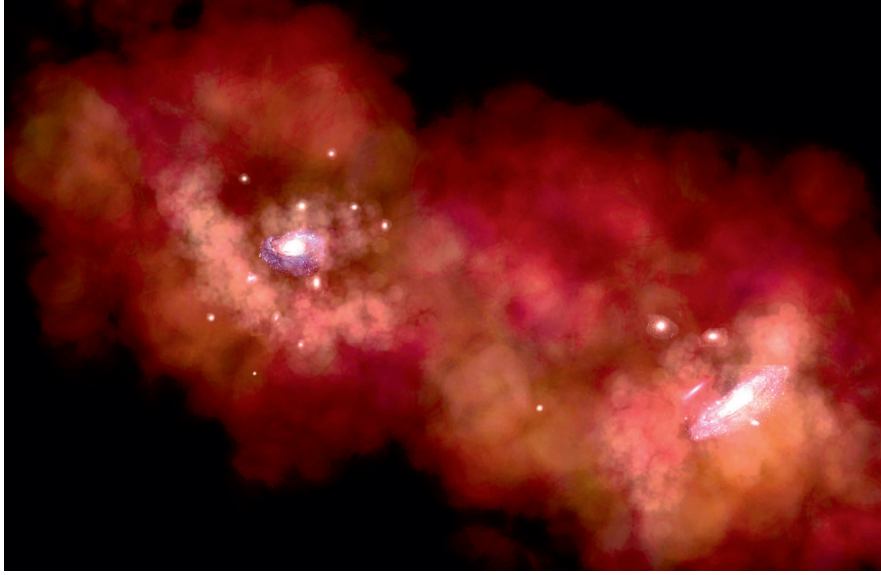


Fig. 1 Sketch of the expected distribution of galaxies and multi-phase gas in the Local Group from an external vantage point. The Milky Way (left big galaxy) and M31 (right big galaxy) are surrounded by their populations of satellite galaxies and by large amounts of multi-phase gas. Both galaxies are interconnected by a gaseous bridge, which spatially falls together with the Local Group barycenter (see, e.g., N14). Figure produced by the author for this review article.

simulations. Finally, it is important to keep in mind that the Milky Way is not an isolated galaxy, but is embedded in the Local Group, being close to another galaxy of similar mass, M31. The original distribution of gas that is entering the virial radius of the Milky Way from outside thus depends on the spatial distribution of satellite galaxies and the distribution of intragroup gas in the cosmological filament that builds the Local Group. In Fig. 1 we sketch the local galaxy distribution in the Local Group and the gas distribution around the Milky Way and M31 from a hypothetical external vantage point.

Turning back to the Milky Way, we know that since $z = 1$ the Milky Way has produced $\sim 8 \times 10^9 M_{\odot}$ of stars, while the current star-formation rate of the Milky Way is $\sim 0.7 - 2.3 M_{\odot} \text{ yr}^{-1}$ (Levine, Blitz & Heiles 2006; Robitaille & Whitney 2010; Chomiuk & Povich 2011; see also Peek 2009). To relate this stellar mass and star-formation rate to the gas-accretion rate it is important to remember that as much as 50 percent of the initial material from which a generation of stars is formed will be returned back to the ISM and will be recycled in later stellar generations (Rana 1991). This means that for one accreted mass unit of gas, *two* mass units of *evolved* stars will have emerged after several star-formation cycles. For the Milky Way, this implies that it has accreted a gas mass of $\geq 4 \times 10^9 M_{\odot}$ during the last 8 Gyr.

1.3 Parameterization of gas accretion

Before we start to discuss in detail the various observational and theoretical aspects of gas-accretion processes in the Milky Way, we need a proper definition of the most important parameters involved, in particular the accretion *rate*. From a cosmological perspective (e.g., in studies using cosmological simulations), the growth and evolution of galaxies through cosmic times is governed by the gain of gas mass within their gravitational sphere of influence (i.e., within their virial radius, R_{vir}) through mergers and gas infall. In this context, one can simply define the gas accretion rate of a galaxy as the net mass inflow of gas through an imaginary sphere with radius R_{vir} . From a galaxy-evolution perspective, in contrast, the only relevant accretion rate is that of the disk, where the infalling gas is being transformed into stars, while the total amount of gas cycling within the galaxy's extended halo is relatively unimportant. One of the most burning questions in gas accretion research therefore is, how much of the gas entering the virial radius of a Milky-Way type galaxy actually makes it to the disk and what are the typical timescales for this process?

In the following, we address these conceptual issues in two steps. First, we define the overall *current-day gas-accretion rate* of the Milky Way simply by relating the total mass of infalling gas, M_{gas} , with its infall velocity, v_{infall} , and its galactocentric distance, d , so that

$$\frac{dM_{\text{gas,halo}}}{dt} = \frac{M_{\text{gas}} v_{\text{infall}}}{d}. \quad (1)$$

Because of the cloud's passage through the halo and the interaction with the ambient hot coronal gas, only a fraction of this initial gas mass will end up in the disk to power star-formation therein. The *future* disk gas accretion rate thus can be defined as

$$\frac{dM_{\text{gas,disk}}}{dt} = \eta \frac{dM_{\text{gas,halo}}}{dt}, \quad (2)$$

where $\eta \leq 1$ represents the *fueling parameter* that modulates the disk's gas accretion and star-formation rate at the time of impact. The accretion time of each infalling gas cloud from its initial position seen today to the disk is $t_{\text{acc}} = d/\langle v_{\text{infall}} \rangle$. Here, $\langle v_{\text{infall}} \rangle$ represents the average infall velocity along the cloud's passage towards the disk. In conclusion, it is the today's 3D distribution and space motion of gas around the Milky Way (parameterized by the current-day halo gas-accretion rate) that governs the *future* star-formation activity in the Milky Way disk.

From equations (1) and (2) it becomes immediately clear, which parameters need to be constrained by observations to get an insight into the gas accretion rate of the Milky Way.

- The **total mass of halo gas** that is potentially flowing towards the Milky Way disk needs to be constrained from observations. Such observations need to take into account the huge span in physical conditions such gas might have: from cold neutral gas (that can be observed in H I 21 cm emission) to million-degree

shock-heated gas (potentially visible in X-ray emission and absorption) all relevant circumgalactic gas-phases need to be considered. Next to sensitivity issues, disentangling distant halo gas from foreground disk gas is difficult for material that has low radial velocities similar to those expected for the rotating interstellar gas disk.

- Also the **distance** of extraplanar/circumgalactic gas needs to be determined by observational means. Reliable distance estimates for gas complexes in the Milky Way halo are particularly challenging. The so-called bracketing method requires the presence foreground and background stars with known distances in the general direction of a halo gas cloud to pinpoint a distance range for it (Prata & Wallerstein 1967). If high-velocity absorption of a given ion is observed in the spectrum of a star with distance d_{star} , it is clear that the absorbing gas is in front of the star at $d_{\text{gas}} < d_{\text{star}}$. The *significant* absence of absorption (for instance, taking into account the absorption strength predicted from the 21 cm emission spectrum) instead implies that the gas lies behind the star. This bracketing method is, however, limited to large, spatially extended gas complexes and requires a substantial observational effort. Other (indirect) distance estimates for extraplanar/circumgalactic gas features (e.g., from modeling the observed $\text{H}\alpha$ fluxes) are afflicted with systematic uncertainties.
- The **infall velocity** of Milky Way halo gas cannot be observed directly, but must be estimated from theoretical considerations in combination with observational constraints. This is because the observed radial velocities, v_{rad} , of extraplanar/circumgalactic gas features do not reflect their 3D space velocities. Also, the effect of galactic rotation adds another velocity component that needs to be taken into account for the interpretation of v_{rad} . As infalling gas is expected to interact with its ambient medium, the infall velocity is likely to depend on the overall halo-gas properties and the position of the infalling gas cloud in the Milky Way potential well, i.e., on its distance to the disk.
- The **fueling parameter** η can only be estimated from full-fledged hydrodynamical models that realistically describe the passage of neutral and ionized gas through the hot coronal gas of the Milky Way. Such models need to take into account the initial gas distribution of the infalling and ambient medium and all relevant physical processes (e.g., instabilities, turbulent mixing layers, conductive interfaces, and many others). In addition, possibly existing *outflowing* gas components (e.g., from SN feedback) are likely to be important.

In the following sections, we will discuss our understanding of these individual parameters in detail, summarizing past and recent observational and theoretical studies.

2 The observed distribution of gas around the Milky Way

To pinpoint the 3D distribution of gas around the Milky Way and to estimate its total mass, the different gas *phases* (in the density-temperature phase-space) need to

be considered. In the following, we separate the Milky Way halo gas in three such phases: (1) neutral/molecular gas, (2) warm ionized gas with temperatures $T \leq 10^5$ K, and (3) hot ionized gas with $T > 10^5$ K. First, we discuss the angular distribution of these phases, their galactocentric distances, and their total mass considering recent observational results. Then, we provide estimates on the gas-accretion rate of the Milky Way based on these observations. Note that many of these aspects have also been discussed in previous reviews (Wakker & van Woerden 1997; Richter 2006; Putman, Peek & Joung 2012) and in the book on HVCs (van Woerden et al. 2004).

2.1 Neutral gas

As discussed earlier, radio observations in the HI 21 cm line have become the most powerful method to study the distribution and internal structure of neutral halo clouds (Bajaja et al. 1985; Hulsbosch & Wakker 1988; Wakker & van Woerden 1991; Hartmann & Burton 1997; Morras et al. 2000; Kalberla et al. 2005; McClure-Griffiths et al. 2009; Winkel et al. 2010). Absorption-line measurements against bright extragalactic background sources (e.g., quasars) provide additional information on the chemical composition of the neutral gas and its connection to the other circumgalactic (ionized) gas phases.

In Fig. 2 we show the sky distribution of the 21 cm IVCs (upper panel) and HVCs (lower panel) plotted in galactic coordinates in an Aitoff-projection centered on $l = 180^\circ$. Because of their different kinematics and intrinsic properties, it is useful to discuss the properties of 21 cm IVCs and HVCs individually.

2.1.1 IVCs

The sky distribution of IVCs indicates that intermediate-velocity gas has predominantly negative radial velocities. The most prominent IVC features (see labels in Fig. 2) are in the northern sky the IV Arch and its low-latitude extension (LLIV Arch), IV Spur, the low-velocity part of Complex L, Complex K, and the low-velocity part of the Outer Arm. In the southern sky, there is the Anticenter (AC) shell and the Pegasus-Pisces (PP) Arch (see Kuntz & Danly 1996; Wakker 2001). The total sky covering fraction of neutral IVC gas is $f_c \approx 0.30$ for column densities $N(\text{HI}) \geq 10^{19} \text{ cm}^{-2}$ and deviation velocities $|v_{\text{dev}}| = 30 - 90 \text{ km s}^{-1}$ (Wakker 2004; see caption of Fig. 2). Many of the IVC features are spatially and kinematically connected with 21 cm disk gas. The typical HI column densities in IVCs in the 21 cm surveys lie in the range $N(\text{HI}) = 10^{19} - 10^{20} \text{ cm}^{-2}$, but some cores in the IV Arch and the Outer Arm exhibit column densities above 10^{20} cm^{-2} (Fig. 2). At positive radial velocities, there is the low-velocity extension of HVC Complex WA in the north and Complex gp in the south. The positive velocity IVCs are much smaller in angular size and column density and they exhibit a very complex internal structure.

Direct distance measurements (mostly using the bracketing technique) place the IVCs relatively close to the Milky Way disk with z heights < 2.5 kpc, typically. The most massive IVC complexes, for example, have distances of $0.8 - 1.8$ kpc (IV Arch), ~ 0.9 kpc (LLIV Arch), and $0.3 - 2.1$ kpc (IV Spur; see IVC compilations by Wakker 2001, 2004 and references therein). Most of the IVCs thus belong to the disk halo interface, which possibly represents a crucial component for gas accretion processes in the Galaxy, as will be discussed below. For the most prominent, large-scale IVC complexes, the 21 cm data indicate individual H I masses on the order of $1 - 8 \times 10^5 M_\odot$ (e.g., IV Arch, LLIV Arch, IV Spur; Wakker 2001). The total neutral gas mass of the large-scale IVCs thus can be estimated to be $\sim 10^6 M_\odot$.

Absorption-line measurements indicate that the metallicity of most of the large northern IVCs is relatively high with typical values between 0.5 and 1.0 solar (e.g., Wakker 2001; Richter et al. 2001a, 2001b). For the Outer Arm, Tripp & Song (2012) derive a lower metallicity of $0.2 - 0.5$ solar, suggesting that this gas (albeit being close to the disk) might have an extragalactic origin, such as many HVCs (see below). Another interesting feature is the core IV 21, which has a metallicity of just 0.4 solar (Hernandez et al. 2013) at a z height of ~ 300 pc above the disk, thus also pointing toward an extragalactic origin. Dust is also present in IVCs, as is evident from the observed depletion patterns of heavy elements in intermediate-velocity gas (Richter et al. 2001a, 2001b; Wakker 2001; see also Savage & Sembach 1996) and from the observed excess of extra-planar infrared emission in the direction of IVCs (Desert et al. 1988, 1990; Weiss et al. 1999). Also molecules (H_2 , CO) have been detected in several IVCs (Richter et al. 2001b, 2003; Wakker 2006; Gillmon et al. 2006; Hernandez et al. 2013; Röhser et al. 2016), but the molecular gas fraction is very small, so that the molecular phase does not contribute significantly to the overall IVC masses. Yet, the presence of molecular gas implies the presence of substantial small-scale structure in the gas down to AU scales (Richter, Sembach & Howk 2003). Small-scale structure is also evident from high-resolution 21 cm data, which show, next to the coherent large-scale 21 cm IVC complexes, a population of several thousand compact H I clumps at $z = 1 - 2$ kpc (e.g., Lockman 2002; Kalberla & Kerp 2009; Saul et al. 2012). These clumps, that have very small masses of only $10^1 - 10^4 M_\odot$, may represent cloudlets that have condensed out of the ambient multi-phase medium. They are raining down to the disk, thus fueling it. Because of their small cross section for absorption spectroscopy, the metal and dust content of these clumps remains unknown so far.

In view of the measured overall chemical composition of the large IVCs and their location in the disk-halo interface, the favored scenario for the origin of near solar-metallicity IVCs is, that these structures represent the back-flow of cooled gas from the galactic fountain process (Shapiro & Field 1976; Houck & Bregman 1990); i.e., they originate from metal-enriched gas that has been ejected from the disk by supernova explosions that is now cycling back to the disk due to gravitational forces.

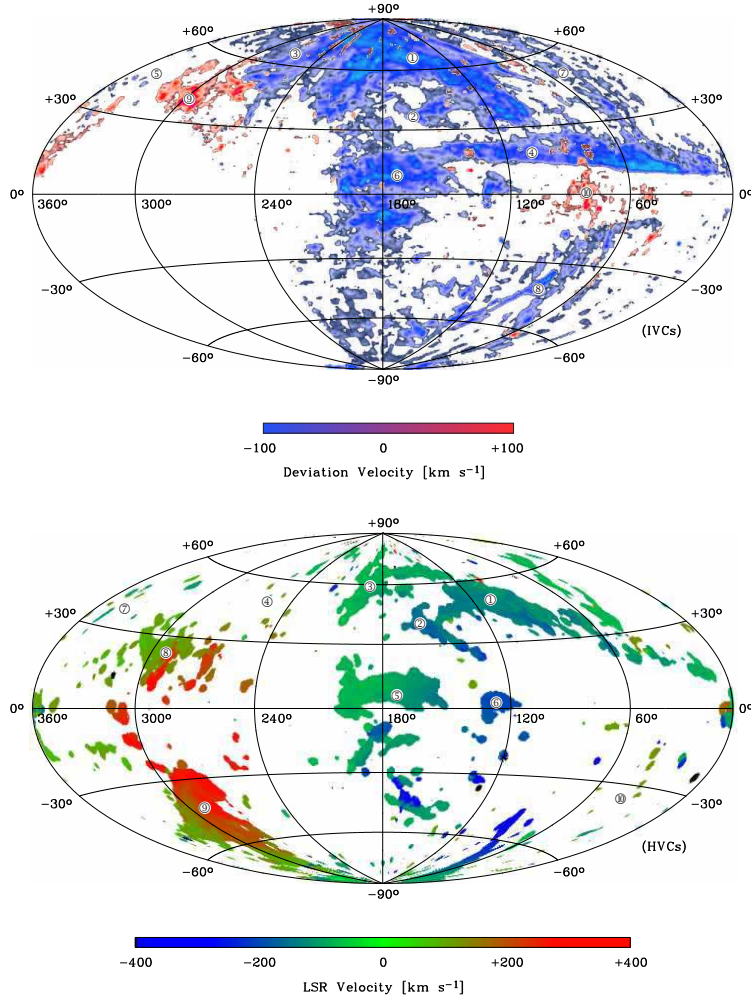


Fig. 2 All-sky maps of 21 cm emission for intermediate-velocity gas (upper panel) and high-velocity gas (lower panel) in an Aitoff projection centered on $l = 180^\circ$. The maps show the sky distribution of neutral gas in the Galactic halo. The maps have been generated from different data sets described in Wakker (2004), Kalberla et al. (2005), and by Tobias Westmeier (priv. comm.). For the IVCs we show (color-coded) the deviation velocity of the gas from a simple model of Galactic rotation (see Wakker 2004) in the range $|v_{\text{dev}}| = 30 - 90 \text{ km s}^{-1}$. For the HVCs, we display the color-coded LSR velocity ($|v_{\text{LSR}}| = 100 - 500 \text{ km s}^{-1}$). Individual neutral IVC and HVC complexes (see Wakker 2001, 2004) are labeled with numbers. For IVCs: (1) IV Arch, (2) LLIV Arch, (3) IV Spur, (4) Outer Arm, (5) Complex L, (6) AC Shell, (7) Complex K, (8) PP Arch, (9) IV-WA, (10) Complex gp. For HVCs: (1) Complex C, (2) Complex A, (3) Complex M, (4) Complex WA, (5) AC Cloud, (6) Complex H, (7) Complex L, (8) Leading Arm of MS, (9) Magellanic Stream, (10) Complex GCN.

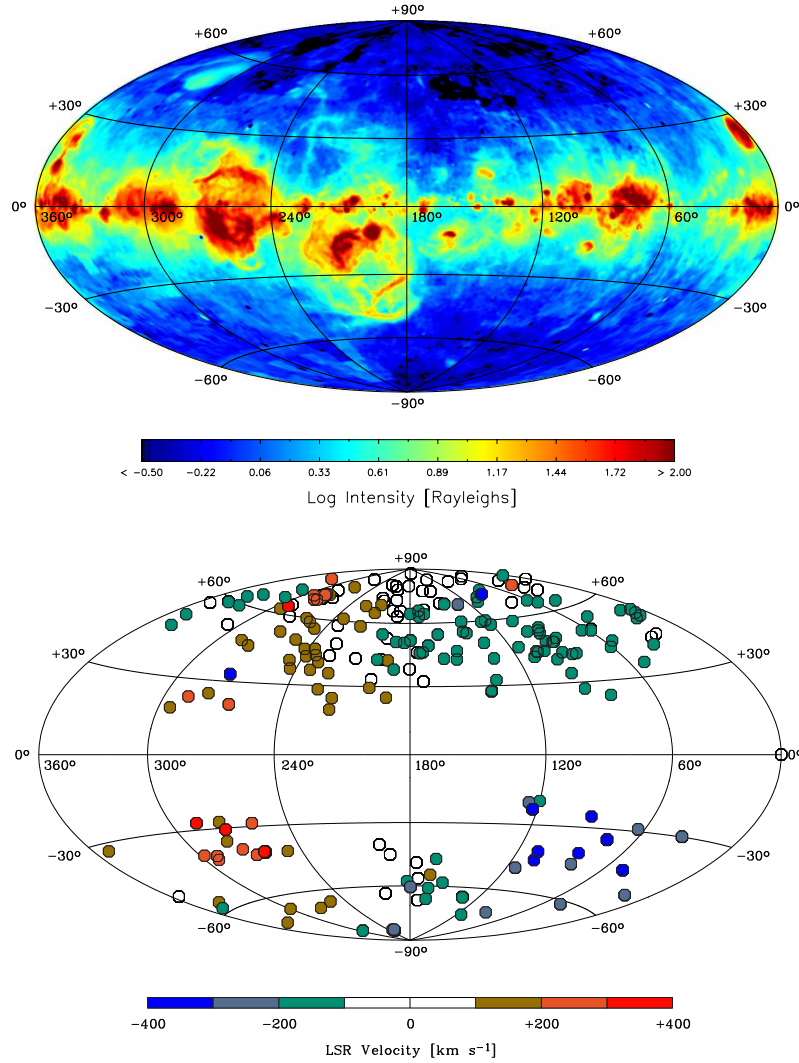


Fig. 3 All-sky maps of H α emission in the Milky Way (upper panel) and high-velocity UV absorption of Si III absorption (lower panel) in an Aitoff projection centered on $l = 180^\circ$. The maps show the sky distribution of diffuse ionized gas (DIG) in the lower and upper Galactic halo, respectively. The H α map (kindly provided by Matt Haffner) has been compiled from data of the Wisconsin H α mapper (WHAM; Haffner et al. 2003, 2016). It shows emission from relatively dense gas that predominantly resides in the inner halo and disk-halo interface of the Milky Way (DIG layer; Reynolds 1991). The Si III data stem from the high-velocity ($|v_{\text{LSR}}| = 100 - 500 \text{ km s}^{-1}$) UV absorption survey from Richter et al. (2017; hereafter referred to as R17) using 265 HST/COS spectra of extragalactic background sources. Diffuse ionized gas has a substantially larger sky covering fraction ($\sim 2 - 3$ times higher) than the neutral gas (Fig. 2).

2.1.2 HVCs

The sky distribution of the Milky Way HVCs is far more complex than that of the IVCs (Fig. 2, lower panel); HVCs span a huge LSR velocity range of $\sim 700 \text{ km s}^{-1}$.

Among the most prominent Milky HVCs is Complex C, which covers ~ 1500 square-degree on the northern sky in 21 cm emission, which is about 4 percent of the entire sky (Wakker 2004). Complex C is a cloud that presumably is being accreted from the IGM or from a satellite galaxy (e.g., Sembach et al. 2004). Another prominent 21 cm HVC is the Magellanic Stream (MS) in the south. The MS also covers an area of ~ 1500 square-degree in 21 cm, but it spreads over the entire southern sky, forming a coherent stream of neutral gas (D’Onghia & Fox 2016). The MS represents a tidal feature expelled from the Magellanic Clouds as they approach the Milky Way halo (e.g., Gardiner & Noguchi 1996; Connors et al. 2006; Besla et al. 2010, 2012; Nidever et al. 2010; Diaz & Bekki 2011, 2012). Over its entire body the MS spans a distance range of $d = 50 - 100$ kpc (or even further) from the Galactic disk, suggesting that it extends over several hundred kpc in the outer halo of the Milky Way (Putman et al. 1998, 2003; Stanimirovic et al. 2002, 2008; Brüns et al. 2005). Other prominent Galactic HVCs are Complex A, Complex H, the Anti-Center Cloud, and Complexes WA–WE. Their positions are indicated in Fig. 2. The individual properties of all HVC complexes are discussed in detail in Wakker (2001).

The entire HVC population of the Milky Way shown in Fig. 2 has a total sky covering fraction in 21 cm of $f_c \approx 0.35$ for neutral gas column densities $N(\text{HI}) \geq 7 \times 10^{17} \text{ cm}^{-2}$ (Murphy, Lockman & Savage 1995; Wakker 2004 and references therein). The covering fraction reduces to $f_c \approx 0.15$ for larger column densities $N(\text{HI}) \geq 2 \times 10^{18} \text{ cm}^{-2}$. The HI column densities in HVCs follow a well-defined column-density distribution function of the form $f(N_{\text{HI}}) \propto N_{\text{HI}}^{-\beta}$ with $\beta = 1.42$ for $\log N(\text{HI}) \geq 18$ (Lockman et al. 2002). With the exception of the MS, all HVCs for which direct distance information from the bracketing method is available, are located within 20 kpc. For instance, the Complexes A & C have distances $d \approx 10$ kpc (van Woerden et al. 1999; Wakker et al. 2007; Smoker et al. 2011; Thom et al. 2008), the Cohen Stream and Complex GCP are at $d = 5 - 15$ kpc (Wakker et al. 2008), and the HVC towards the LMC has $d \approx 9$ kpc (Richter et al. 2015). For these structures in the inner Milky Way halo the distances estimated indirectly from the measured $\text{H}\alpha$ fluxes agree well with the values derived from the bracketing method (e.g., Bland-Hawthorn & Putman 2001; Putman et al. 2003; Tufté et al. 2002). Combining the 21 cm emission in Milky Way HVCs and in M31 halo clouds, Richter (2012) predicts that the HI covering fraction in HVCs around Milky Way-type galaxies declines exponentially with galactocentric distance with $f_c < 0.01$ for $d > 70$ kpc. From deep 21 cm observations of the M31 halo (Westmeier et al. 2007) further follows that also the so-called compact high-velocity clouds (CHVCs), isolated high-velocity 21 cm gas clumps with very small angular sizes of < 2 deg (Braun & Burton 1999; de Heij, Braun & Burton 2002), are located at $d < 50$ kpc, disproving a previous scenario in which CHVCs are regarded as gas-filled dark matter halos residing in the Local Group (Blitz et al. 1999; Braun & Burton 1999).

From the 21 cm data and the available distance information it follows that the total neutral HVC gas mass is $M_{\text{HI,HVC}} \approx 2.5 \times 10^8 M_{\odot}$ (Wakker 2004; Brüns et al. 2005). The MS contributes with more than 60 per cent to this mass ($M_{\text{HI,MS}} \approx 1.6 \times 10^8 M_{\odot}$ for $d = 55$ kpc), while the other HVCs have substantially smaller masses (e.g., $M_{\text{HI,ComplexC}} \approx 5 \times 10^6 M_{\odot}$; Wakker 2004). Since the two Magellanic Clouds are located at only ~ 80 kpc distance, their interstellar gas content adds to the gas mass being accreted by the Milky Way. Therefore, if we add the neutral gas mass of the Magellanic Clouds and their gaseous interconnection, the Magellanic Bridge, the total HI budget in the Milky Way halo sums up to a value of $M_{\text{HI,MW halo}} \approx 1.3 \times 10^9 M_{\odot}$, which is ~ 20 percent of the neutral gas mass in the Milky Way disk ($M_{\text{HI,MW disk}} \approx 7 \times 10^9 M_{\odot}$; Ferriere 2001).

Other tracers of predominantly neutral gas in the Milky Way halo are absorption lines of neutral and low ions, such as O I, N I, Ar I, S II with transitions in the UV, and Ca II and Na I in the optical regime. From a survey of high-velocity Ca II/Na I absorption in the Milky Way halo against several hundred extragalactic background sources, Ben Bekhti et al. (2008, 2012) derive a covering fraction of $f_c \approx 0.50$ for $\log N(\text{Ca II}) > 11.4$, which is ~ 2 times higher than the 21 cm covering fraction. These results further indicate the widespread presence of cold, neutral gas structures away from the large 21 cm complexes. Such structures possibly are too small to be seen in all-sky 21 cm survey because of the limited angular resolution of these surveys in combination with beam-smearing effects.

While most of the IVCs have near-solar metallicities, the metal abundance in many HVCs is substantially lower (by a factor 5 – 10, typically). For Complex C, the (mean) metallicity has been constrained to 0.15 solar (Wakker et al. 1999; Richter et al. 2001a; Tripp et al. 2003; Collins, Shull & Giroux 2003; Sembach et al. 2004). The main body of the Magellanic Stream also has a metallicity of only 0.1 solar (Fox et al. 2010, 2013), but the MS contains a filament that is more metal rich (0.3 solar; Richter et al. 2013; Gibson et al. 2001). Similarly, Complex A most likely has metallicity of only ~ 0.1 solar (Wakker 2004). Such low metallicities are in line with the idea that HVCs represent gas infalling from the pre-enriched intergalactic medium (or intragroup gas), but the clouds may also trace material stripped from satellite dwarf galaxies as they are being accreted by the Galaxy. Moreover, it cannot be ruled out that some of the gas has been part of the Milky Way a long time ago, then was ejected (at relatively low metallicity) by a former Galactic outflow or wind, and now is raining back towards the disk (“intergalactic fountain”). An example for this latter scenario is the Smith Cloud (also called Complex GCP), which has a metallicity of 0.5 solar and is believed to originate in the outer Galactic disk (Lockman et al. 2008; Hill, Haffner & Reynolds 2009; Fox et al. 2016).

There appears to be only little dust in neutral and ionized HVCs (e.g., Wakker & Boulanger 1986; Bates et al. 1988; Tripp et al. 2003; Richter et al. 2001, 2009; Williams et al. 2012). The few tentative detections of far-IR emission in some HVCs (e.g., Miville-Deschênes et al. 2005; Peek et al. 2009; Planck Collaboration 2011) remain inconclusive with respect to their dust abundance. Diffuse molecular gas is present only in high-column density regions of the Magellanic Stream (Sembach et al. 2001; Richter et al. 2001c, 2013), the Magellanic Bridge (Lehner 2002; Murray

et al. 2015), and in a dense clump of an HVC projected onto the LMC (Richter et al. 1999). However, the molecular component is not of importance for the total mass of HVCs.

Finally, it is worth noting that some of the above mentioned neutral halo clouds (e.g., Complex L) exhibit a radial velocity range that extends from values below 100 km s^{-1} to values above this threshold, i.e., these complexes can be regarded as *both* IVCs and HVCs, although they each represent a single, kinematically coherent structure. The question arises, whether the separation of IVCs and HVCs as different halo-cloud populations is justified, or whether they just represent the same population of objects with just different radial velocities. As discussed above, distance measurements place the IVCs within 2.5 kpc of the Milky Way disk, while most of the HVCs are located much further away. This, together with the on average higher metallicity of IVCs compared to HVCs, indeed indicates that low-velocity halo clouds (with LSR velocities *typically* $< 100 \text{ km s}^{-1}$) predominantly reside in the disk-halo interface, while high-velocity halo clouds (with LSR velocities *typically* $\geq 100 \text{ km s}^{-1}$) predominantly trace gas at $d = 2 - 100 \text{ kpc}$.

2.2 Warm ionized gas

Warm ionized gas in the Milky Way halo is even more widespread than the neutral gas traced by 21 cm emission. We here define warm-ionized gas as gas that is predominantly ionized (i.e., with small neutral gas fractions) and has a temperature $< 10^5 \text{ K}$. Circumgalactic gas at such temperatures is expected to be photoionized by the combined ionizing radiation from stars in the Milky Way disk and the ambient extragalactic UV background at $z = 0$ (see model by Fox et al. 2005). Warm ionized gas in the Milky Way halo can be detected either in emission in recombination lines such as $\text{H}\alpha$ or in high-velocity UV absorption of so-called intermediate ions that have lower ionization boundaries in the range 15 – 40 eV (e.g., C III, N III; Si III, Si IV, Fe III; Morton 2003; R17).

In Fig. 3, upper panel, we show the sky distribution of $\text{H}\alpha$ emission in the range $0.3 - 100 \text{ Rayleigh}$, based on data obtained from the Wisconsin $\text{H}\alpha$ Mapper (WHAM; Haffner et al. 2003, 2016). As can be seen, $\text{H}\alpha$ emission is widespread at latitudes $b < 30^\circ$, situated in distinct coherent spatial structures such as lobes and arches. These features reflect the complex motions of diffuse ionized gas (DIG) in the disk-halo interface (DHI) that is believed to be shaped by the on-going star-formation in the Milky Way disk. Based on the derived gas densities and volume filling factors (Reynolds et al. 2012; Haffner et al. 2003), the total mass of ionized gas in the DHI of the Milky Way can be estimated to be $\sim 10^8 M_\odot$, in line with estimates for extra-planar ionized gas in other low-redshift disk galaxies (e.g., NGC 891; Dettmar 1990).

Many of the 21 cm HVCs at much larger distances from the disk are also detected in $\text{H}\alpha$ emission (e.g., Weiner & Williams 1996; Tufté, Reynolds & Haffner 1998; Bland-Hawthorn et al. 1998), indicating that the neutral gas clouds are surrounded

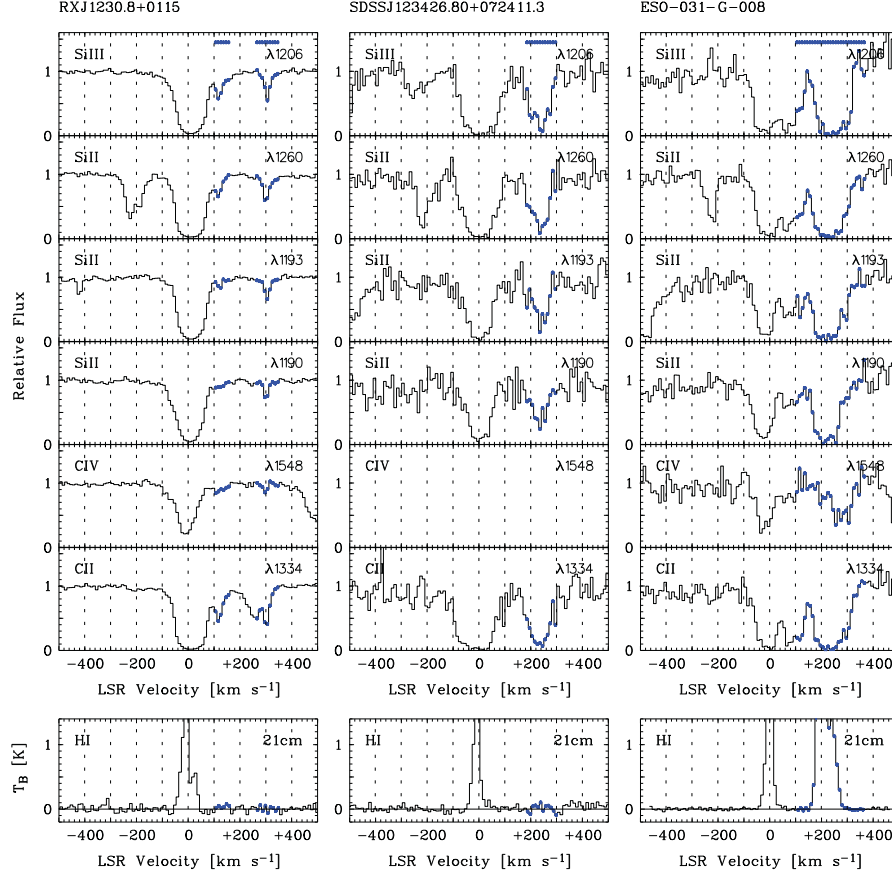


Fig. 4 Velocity profiles of high-velocity UV absorbers in the Galactic halo along three lines of sight (from R17), based on HST/COS data. Absorption profiles of various transitions from Si III, Si II, C IV, and C II are shown, where the high-velocity absorption at $|v_{\text{LSR}}| \geq 100 \text{ km s}^{-1}$ is indicated in blue. We also show the H I 21 cm emission profiles (from GASS/EBHIS data) for the same sightlines in the lowest panels. The individual high-velocity absorption features towards RXJ1230.8+0115 and SDSSJ123426.80+072411.3 trace gas streams in the halo that are predominantly ionized (without H I 21 cm counterpart), while the high-velocity absorption towards ESO-031-G-008 traces neutral *and* ionized halo gas related to the MS (UV absorption plus H I 21 cm emission).

by envelopes of ionized gas, whose masses are comparable with or even larger than the neutral gas body (e.g., Fox et al. 2004). Also the Magellanic Stream at $d = 50 - 100 \text{ kpc}$ is detected in H α (e.g., Putman et al. 2003; Fox et al. 2014), proving that the MS is surrounded by substantial amounts of warm H II. From the models of Bland-Hawthorn et al. (2007) it follows that the mass-weighted H II column density in the MS is $> 10^{20} \text{ cm}^{-2}$, thus larger than the mass-weighted H I column density. A similar conclusion was drawn by Fox et al. (2014), who determine an ionized-to-

neutral hydrogen mass ratio of ~ 3 based on the absorption strength of intermediate and high ions associated with the 21 cm body of the Stream.

The most sensitive ions to trace the warm ionized gas in the halo are C III and Si III with strong transitions in the UV at 977.02 Å (C III) and 1206.50 Å (Si III; see Richter et al. 2016). In their recent legacy survey of high-velocity UV absorption in the Milky Way halo, R17 found that warm ionized halo gas, as traced by Si III at velocities $|v_{\text{LSR}}| \geq 100 \text{ km s}^{-1}$ and column densities $\log N(\text{Si III}) \geq 12.1$, has a covering fraction as high as $f_c = 0.74$, confirming earlier results based on much smaller samples (Collins, Shull & Giroux 2009; Shull et al. 2009; Lehner et al. 2012; Herenz et al. 2013). This covering fraction is more than twice the value obtained for the neutral HVCs from the 21 cm observations (see above). In the lower panel of Fig. 3 we show the sky distribution of high-velocity Si III absorption, which can be directly compared with the 21 cm HVC map (Fig. 2, lower panel). Like the H α emission, high-velocity Si III absorption is often associated in radial velocity with the 21 cm HVC features, even if located several degrees away from the 21cm contours. This further implies that HVCs represent coherent multi-phase gas streams (with a neutral gas body surrounded by an ionized gas layer) that move through the Milky Way halo (Lehner et al. 2012). Figs. 2 and 3 also indicate that there are several regions in the high-velocity sky that exhibit pronounced Si III absorption but do not show significant large-scale H I. In contrast to the 21 cm HVCs and their ionized envelopes, gas in these regions can be regarded as *coherent ionized gas streams* in which patchy condensations of cooler, neutral gas clumps are embedded. Particularly interesting are the regions $l > 200^\circ, b > 0^\circ$ and $l < 120^\circ, b < 0^\circ$, which form a velocity dipole on the sky in UV absorption (Fig. 2; R17; Collins, Shull & Giroux 2003) in a direction that forms the major axis of the Local Group cosmological filament (N14). The observed kinematically distinct absorption features at high positive and high negative radial velocities possibly indicate that the Milky Way is ramming into ionized intragroup gas because it follows the general flow of galaxies in the direction of the Local Group barycenter (Peebles et al. 2001, 2011; Whiting 2014), while it is moving away from Local Group gas in the opposite direction along the filament (R17). Therefore, the Milky Way’s accretion of warm ionized gas might be strongly influenced by the local galaxy environment and cosmological structure formation in the Local Group (N14). This important aspect will be further discussed in Sect. 3.2.

The ionized gas components that are associated with the 21 cm features obviously have the same distances as the neutral halo clouds. They also have comparable metallicities, if the gas has not yet been mixed with the ambient hot coronal gas. This implies that the majority of the diffuse ionized halo clouds that are *not* associated with the MS are located at $d < 20 \text{ kpc}$, while the ionized envelope of the Stream is at $d = 50 - 100 \text{ kpc}$. The exact angular extent of the Stream’s ionized gas component is unknown, but it may well cover 30 – 50 percent of the entire sky (R17; Fox et al. 2014). From their survey of high-velocity UV absorption towards Galactic halo stars with known distances ($d < 15 \text{ kpc}$) and extragalactic background sources Lehner & Howk (2011) and Lehner et al. (2012) find that the sky-covering fraction of high-velocity UV absorption increases only marginally from the halo-star sample to the QSO sample, if velocities $|v_{\text{LSR}}| \leq 170 \text{ km s}^{-1}$ are considered.

This indicates that HVCs in this velocity range are predominantly located at $d < 15$ kpc. In contrast, HVCs with absolute LSR velocities larger than 170 km s^{-1} (e.g., the MS) are only seen against extragalactic background sources, demonstrating that the gas is located at $d > 15$ kpc, and being in line with the distance constraints for the neutral gas (see above). The halo-star sample of Lehner & Howk (2011) and Lehner et al. (2012) covers only a limited fraction of the sky, however, so that the possible presence of more distant ionized gas structures even at low velocities (in particular in the directions of a possible Local Group filament) cannot be ruled out with these data.

The total mass of diffuse ionized high-velocity gas in the Galactic halo is dominated by the extended envelope of the MS (Fox et al. 2014; R17). Assuming $d = 55$ kpc and calculating the amount of H II from the observed ion abundances in combination with an ionization model, both studies obtain a gas mass of the ionized component of the MS of $M_{\text{MS}} \approx 1 - 3 \times 10^9 M_{\odot}$. This mass would be substantially higher, if some of the gas from the MS was located at larger distances. For instance, if the distance of MS would lie in the range $d = 100 - 150$ kpc (see Besla, et al. 2012; Jin & Lynden-Bell 2008; Bland-Hawthorn et al. 2013), the mass of the ionized component of the MS would be as large as $\sim 3 - 7 \times 10^9 M_{\odot}$, thus very close to the total ISM gas mass in the Galactic disk (Ferriere 2001). The contribution of high-velocity absorbers at $d < 20$ kpc to the ionized gas mass in the halo is small instead; their gas mass sums up to a total value of no more than $M_{\text{HVCs}, d < 20 \text{ kpc}} = 2 \times 10^7 M_{\odot}$ (R17). This value still is comparable to or even higher than the mass of the neutral gas in the same distance range.

2.3 Hot ionized gas

Ever since the prediction of Lyman Spitzer in 1956 on the existence of a Galactic Corona (see Sect. 1), the search for a low-density, high-temperature ($T > 10^5$ K) gaseous medium that surrounds the Milky Way has been of high priority for astrophysicists, as the Corona links the observed properties of the Galaxy to cosmological structure formation (see, e.g., Oort 1966). From more recent theoretical work (e.g., Maller & Bullock 2004), it is indeed expected that all MW-type galaxies are surrounded by massive, hot gaseous halos of typical mass of $10^{11} M_{\odot}$ and temperature $T \sim 10^6$ K (the virial temperature of the galaxy's DM halo). If some fraction of the gas was able to cool, it would sink towards the disk, feeding the galaxy with fuel for future star formation. Therefore, hot coronal gas may serve as a huge baryon reservoir from which MW-type galaxies gain their gas. In addition, the hot Milky Way halo might be further fed with gas from a possible large-scale outflow from the Galactic center region (Fox et al. 2015; Lehner et al. 2012; Zech et al. 2008; Bland-Hawthorn & Cohen 2003; Su, Slayter & Finkbeiner 2010).

Despite the obvious importance of the hot, ionized circumgalactic gas phase for galaxy evolution, our knowledge about the properties and spatial extent of hot coronal gas in the Milky Way still is very limited. This is because it is very difficult

to detect such coronal gas that is expected to have very low densities ($n_{\text{H}} < 10^{-3} \text{ cm}^{-3}$), in particular in the outer regions of the halo. Observational evidence for the existence of a hot Milky Way Corona comes from observations in the X-ray regime, where the gas can be observed in emission or in absorption against extragalactic X-ray point sources. Using ROSAT data, Kerp et al. (1999) systematically searched for X-ray emission spatially associated with neutral HVCs and reported several positive detections, e.g., in the direction of Complex GCN, Complex C, and Complex D. In Fig. 5, we show as an example the ROSAT emission map of hot halo gas in the direction of Complex GCN from the study of Kerp et al. Other observations of the soft X-ray background support the existence of hot coronal gas in the Milky Way (e.g., Kuntz & Snowden 2000). X-ray absorption of O VII and O VIII in the Galactic halo has been reported by several groups (Wang et al. 2005; Fang et al. 2002, 2003, 2006; Mathur et al. 2003; Bregman 2007; McKernan, Yaqoob & Reynolds 2004; Williams et al. 2005; Gupta et al. 2012; see also Miller, Kluck & Bregman 2016), but the interpretation of these low-resolution spectra is afflicted with systematic uncertainties (see Richter, Paerels & Kaastra 2008). Also pulsar dispersion measures have been used to constrain the properties of hot coronal gas in the Milky Way halo (e.g., Gaensler et al. 2008). All these observations are biased towards the regions with the highest gas densities in the Corona, however, so that the bulk of the hot gas detected in this manner presumably resides in the inner halo at $d < 20$ kpc (e.g., Rasmussen et al. 2003). It therefore remains unknown whether the coronal gas really extends to the virial radius of the Milky Way ($R_{\text{vir}} \sim 260$ kpc; e.g., Tepper-García et al. 2015) and how it connects to gas gravitationally bound to the Local Group. From the UV observations of O VI in the thick disk of the Milky Way (Widmann et al. 1998; Savage et al. 2003; Wakker et al. 2003; Savage & Wakker 2009) indeed follows that there are large amounts of extra-planar warm-hot gas at vertical heights $z < 5$ kpc.

Indirect evidence for the widespread presence of hot gas in the Milky Way halo comes from the many UV absorption-line detections of *high-velocity* O VI (Sembach et al. 2003; Wakker et al. 2003), which has a sky covering fraction as large as $f_{\text{c}} = 0.60 - 0.85$. O VI arises in warm-hot gas at $T \sim 3 \times 10^5$ K and is believed to trace the interface regions between the hot coronal gas and cooler halo clouds embedded therein (i.e., the neutral and ionized HVCs; see above). Isolated, strong O VI absorption at high velocities is also seen in the direction of the Local Group barycenter and, in particular, towards the quasar Mrk 509 in HVC Complex GCN (Fig. 5), where enhanced X-ray emission and high-velocity Si III absorption is observed (Collins, Shull & Giroux 2005; see above). The coincidence of UV absorption and X-ray emission further indicates that there is an excess of hot gas in this direction that possibly is related to highly-ionized intragroup gas near the Local Group barycenter, towards which the Milky Way is moving (see Sect. 2.2).

To estimate the baryon content of the Milky Way's coronal gas, its radial density profile needs to be constrained. Due to on-going accretion of gas and stars from satellite galaxies and the IGM, substantial deviations from a simple hydrostatic density distribution are likely. Even for a hot halo that is not perfectly hydrostatic, however, the average gas density in the coronal gas is expected to decrease

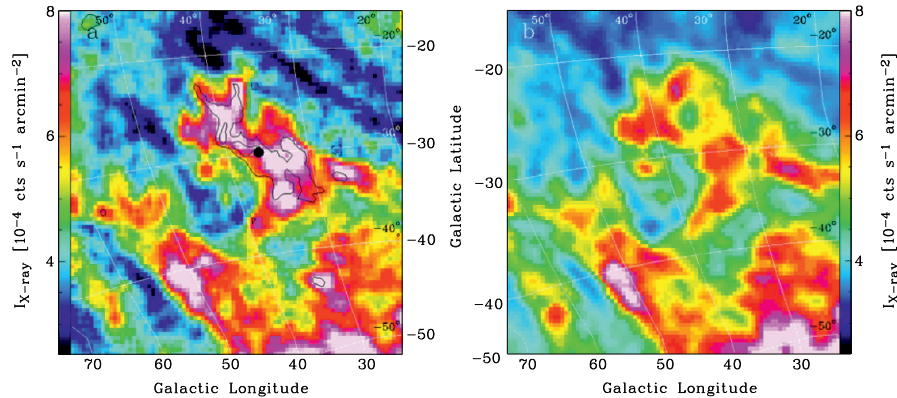


Fig. 5 *Left panel:* X-ray emission map of hot gas in the direction of HVC complex GCN, based on ROSAT 0.25 keV soft-X ray background (SXR) data (see Kerp et al. 1999 for details). The position of the background quasar Mrk 509 is indicated with the black dot. In this direction, hot halo gas has been detected in high-velocity O VI absorption using FUV data (Sembach et al. 2003; see also Winkel et al. 2011). *Right panel:* model of the SXR emission in the same direction, based on 21 cm HI data from foreground gas (causing photoelectric absorption of the background X-ray photons) and assuming a homogenous distribution of the X-ray background (Kerp et al. 1999). Both maps indicate the presence of hot coronal gas in the Galactic halo in this area of the sky. Maps kindly provided by Jürgen Kerp.

for increasing distances to the disk. From X-ray absorption, spectra Bregman & Lloyd-Davies (2007) estimate a gas density of $n_{\text{H}} \approx 8 \times 10^{-4} \text{ cm}^{-3}$ for the inner halo ($d < 20 \text{ kpc}$). From pulsar dispersion measures instead follows that the average coronal gas density must be smaller, $n_{\text{H}} < 8 \times 10^{-4} \text{ cm}^{-3}$, in line with studies that estimate n_{H} indirectly from considering the interaction between the cool HVCs and the ambient hot medium ($n_{\text{H}} \approx 2 \times 10^{-4} \text{ cm}^{-3}$; Grcevich & Putman 2009; Peek et al. 2007; Tepper-Garcia et al. 2015). Because of the unknown extent and the unknown gas properties at the virial radius, the total mass of the Milky Way’s hot coronal gas is very uncertain. For $d < 250 \text{ kpc}$ the total mass is estimated to be $M_{\text{Corona}} \approx 10^{10} - 10^{11} M_{\odot}$ (Anderson & Bregman 2010; Yao et al. 2008; Gupta et al. 2012; Miller & Bregman 2013, 2015; Fang, T., Bullock & Boylan-Kolchin 2013; Salem et al. 2015), in line with the idea, the Milky Way’s hot Corona represents a huge baryon reservoir. However, the hot coronal gas must cool and condense into streams of denser gas to be able to sink to the Milky Way disk, i.e., it must transit through the diffuse ionized and/or neutral phase to contribute to the gas-accretion rate. To understand the details of this important phase transition, hydrodynamical simulations are required, which will be discussed in Sect. 3.

2.4 Gas-accretion rates from observations

The observations presented in the previous sections suggest that HVCs (and IVCs) represent coherent entities of multi-phase gas that move within the Milky Way halo (Lehner et al. 2012; R17). Independent of their individual origin (tidal interactions with satellite galaxies, infall from the IGM or intragroup medium, condensations from the hot coronal gas, the back-flow of material expelled previously from the disk), these streams of gas trigger the Galaxy’s present-day gas-accretion rate as defined in equation (1) and we will discuss their contribution to $dM_{\text{gas,halo}}/dt$ in the following.

While the 3D distribution of neutral and diffuse ionized gas around the Galaxy (i.e., $M_{\text{gas,halo}}, d$) is constrained by observations, the space *motion* of the gas is not, as only the radial component of the velocity can be observed. In lack of further information, the mean infall velocity often is assumed to be constant for all halo clouds, although it is likely that v_{infall} spans a large range for the IVCs and HVCs and systematically depends on d (see Sect. 1). For the MS, recent studies assume $\langle v_{\text{infall}} \rangle = 100 \text{ km s}^{-1}$ (e.g., Fox et al. 2014), a value that also has been used for other HVCs (e.g., Complex C; Wakker et al. 1999, 2008). A more complex model for v_{infall} is presented by Putman, Peek & Joung (2012), where they try to separate for the HVC population the azimuthal velocity component from the accretion velocity in the Galactic center (GC) direction and derive $\langle v_{\text{infall,GC}} \rangle \approx -50 \text{ km s}^{-1}$. This value is consistent with the *mean* radial velocity of HVCs of $\langle v_{\text{rad}} \rangle \approx -50 \text{ km s}^{-1}$, but the most distant halo structures, such as the MS, might have somewhat larger accretion velocities (Mathewson et al. 1974).

Because of its large mass, the MS dominates by far the total present-day gas accretion rate of the Milky Way. From their UV absorption-line survey Fox et al. (2014) derive a mass inflow rate of neutral and diffuse ionized gas from the Stream of $dM_{\text{MS}}/dt \approx 2 M_{\odot} \text{ yr}^{-1}$ for a fixed distance of the MS of $d = 55 \text{ kpc}$ and $\langle v_{\text{infall}} \rangle = 100 \text{ km s}^{-1}$. At this distance and infall velocity, the gas (or better said, a fraction η of it; see equation (2)) would reach the disk in $\sim 540 \text{ Myr}$. If, instead, the distance of the Stream was $d = 100 \text{ kpc}$, then it would take $\sim 1 \text{ Gyr}$ for the gas to reach the disk and the accretion rate would be higher by a factor of ~ 2 , because the estimate of M_{MS} depends on its assumed distance. Taking $d = 55 \text{ kpc}$ as a conservative lower limit and adding the gas mass associated with the Magellanic Clouds and the Magellanic Bridge (with all these components together forming the *Magellanic System*), the total accretion rate from all these components sums up to a value of $dM_{\text{MSys}}/dt \geq 3.7 M_{\odot} \text{ yr}^{-1}$; Fox et al. 2014)

Based on the observed properties discussed above, the contribution of the other *individual*, 21 cm-selected HVC Complexes at $d < 20 \text{ kpc}$ to the mass-inflow rate (including both neutral and ionized gas) is expected to be rather small (e.g., Complex C: $0.1 - 0.2 M_{\odot} \text{ yr}^{-1}$; Complex A: $0.05 M_{\odot} \text{ yr}^{-1}$; Cohen Stream: $0.01 M_{\odot} \text{ yr}^{-1}$; see Wakker et al. 1999, 2007, 2008; Thom et al. 2006, 2008; Putman, Peek & Joung 2012; R17). Putman, Peek & Joung (2012) derive a maximum accretion rate of $0.4 M_{\odot} \text{ yr}^{-1}$ for all HVCs *except* the MS. If we consider only the neutral gas mass in the Galactic HVC population, the total H I gas accretion rate from all 21 cm HVCs

(including the MS) comes out to $dM_{\text{HI}}/dt = 0.7 M_{\odot} \text{yr}^{-1}$ (Richter 2012), again assuming that the MS is at $d = 55$ kpc.

The general distribution of UV-absorbing gas in the halo (and its total mass) yet implies, that the *ionized* component (independent of whether it is associated with H I emission or not) dominates the gas accretion not only for the MS, but also for the nearby HVCs at $d \leq 20$ kpc. From their absorption-line survey towards halo stars and extragalactic background sources, Lehner & Howk (2011) determine an accretion rate of predominantly ionized high-velocity gas at $d < 15$ kpc of $0.45 - 1.40 M_{\odot} \text{yr}^{-1}$. Putting it all together, R17 estimate from their UV absorption-line survey of 265 sightlines a total gas-accretion rate of neutral and ionized high-velocity gas in the halo (including gas from the Magellanic System) of $dM_{\text{HVC}}/dt \geq 5 M_{\odot} \text{yr}^{-1}$. This limit is higher by a factor of > 2 than the *current* star-formation rate of the Milky Way ($\sim 0.7 - 2.3 M_{\odot} \text{yr}^{-1}$; e.g., Robitaille & Whitney 2010; Chomiuk & Povich 2011).

The contribution of the 21 cm IVCs and the DIG in the disk-halo interface (DHI) at z -heights < 2.5 kpc to the Milky Way’s gas-accretion rate is significantly smaller than that of the neutral HVCs. Considering the IVC distances and neutral-gas masses discussed in Sect. 2.1.1, the neutral gas-accretion rate from IVCs is only $\sim 0.01 - 0.05 M_{\odot} \text{yr}^{-1}$. A much higher gas-accretion rate can be determined considering the ionized gas reservoir in the DIG (Sect. 2.2). In principle, the overall gas flow in the DIG of Milky-Way type is expected to be strongly influenced by the various feedback processes from the disk (e.g., radiative and mechanical feedback from supernovae, stellar winds, and AGN; e.g., Bland-Hawthorn & Maloney 2002; MacLow & Klessen 2004; Springel & Hernquist 2005; Marasco, Marinacci & Fraternali 2013), but the exact role of these processes in the gas-circulation cycle of the Milky Way’s DHI is uncertain. Assuming that at least half of the diffuse ionized gas in the disk-halo interface is currently being accreted (the rest being related to outflowing gas), the observational constraints imply $dM_{\text{DHI}}/dt = 1 - 2 M_{\odot} \text{yr}^{-1}$ for $v_{\text{infall}} \leq 20 \text{ km s}^{-1}$, thus in line with the current star-formation rate (see also Fraternali et al. 2013). A net-infall of ionized gas is in line with the observed H α kinematics (Haffner et al. 2003).

Some interesting conclusions can possibly be drawn from these numbers. Obviously, the amount of large-scale *neutral* gas in the disk-halo interface is much smaller than the amount of large-scale neutral gas at larger distances; it is also much smaller than the amount required to keep up the current star-formation rate in the disk. Infalling neutral gas structures thus might be disrupted and ionized when entering the disk-halo interface, where it might re-cool and condense again before it enters the disk. This re-processing of infalling gas in the disk-halo interface is sometimes referred to as “quiet accretion”. The galactic-fountain flow is believed to play a crucial role in the the gas cooling and condensation processes (Marinacci et al. 2010; Armilotta, Fraternali & Marinacci 2016). The infalling gas thus might enter the disk in the form of low-velocity, mildly-ionized gas clumps or tiny 21 cm drops (Lockman 2002; Begum et al. 2010; Ford, Lockman & McClure-Griffiths; see Sect. 2.1), thus in a form that is difficult to identify observationally.

Another possible reason for the apparent discrepancy between the neutral gas budget in the DHI and that at larger distances might be the existence of neutral DHI gas that is “hidden” to us: clouds that have low radial velocities (LVCs; see Sect. 1.1), similar to those in the disk, but that reside in the (lower) Galactic halo (e.g., Zheng et al. 2015; Peek et al. 2009). Finally, also gas from the outer disk might contribute to the fueling of star formation in the inner regions of the Milky Way disk through a *radial* inflow of gas (e.g., Elson et al. 2011; Sellwood & Binney 2002; see also Putman, Peek & Joung 2012 and references therein).

Obviously, observations alone cannot provide a full insight into the complex processes that govern the past, present, and future gas-accretion rate of the Milky Way. Hydrodynamical simulations represent an important toolkit to further study the dynamics and physical properties of gas falling toward Milky-Way type galaxies and to pinpoint the overall mass-inflow rate to the disk. The most relevant of these aspects will be discussed in the following section.

3 Simulations of Milky Way gas accretion

In this section, we briefly discuss results from theoretical studies of accretion processes of Milky Way-type galaxies based on hydrodynamical simulations. Although these studies will also be discussed in a more general context in other chapters in the second part of this book, they are particularly important for our understanding of gas accretion in the Milky Way and thus need to be considered in this review.

3.1 Hydrodynamical simulations of gas infall

Whatever the initial conditions of an infalling gas structure at a given distance to the Galaxy might be, the gas will interact with the ambient hot coronal medium that fills the galaxy’s dark-matter potential. Modeling these interaction processes are of fundamental importance to understand origin and fate of accreted material and to explain the observations discussed in the previous sections.

As mentioned earlier, one plausible scenario for gas accretion in Milky-Way size gaseous halos with $M_{\text{halo}} \sim 10^{12} M_{\odot}$ and $R_{\text{vir}} \sim 250$ kpc is the cooling and fragmentation of hot ($T \sim 10^6$ K) halo gas that falls towards the Galactic disk in the form of overdense clouds (Maller & Bullock 2004). Support for this scenario comes from early SPH simulations (Kaufmann et al. 2006, 2009; Sommer-Larsen 2006). In these simulations, cool pockets of gas condense out from the hot coronal gas from thermal instabilities, mimicking the properties of the Galactic 21 cm HVCs that have $d < 20$ kpc (Peek, Putman & Sommer-Larsen 2008). More recent studies indicate, however, that these early studies may draw a too simplistic picture of the HVC condensation process. One problem lies in the buoyancy of thermally unstable gas, which is expected to disrupt condensing seed structures before they can cool efficiently (Burkert

& Lin 2000). Thus, linear isobaric perturbations in a homogeneous, hot coronal gas are expected to be inefficient to develop cool gas patches in the halo, unless the entropy gradient is very small. An alternative scenario is offered by Joung, Bryan & Putman (2012), who study the condensation process in Galactic coronal gas from non-linear perturbations that might be generated from either infalling intergalactic gas (e.g., Kereš & Hernquist 2009; Kereš et al. 2009; Brooks et al. 2009) or from the gaseous leftovers of satellite accretion (Bland-Hawthorn et al. 2007; Grcevich & Putman 2009; Nichols & Bland-Hawthorn 2011; see below). Joung, Bryan & Putman (2012) find from their high-resolution adaptive mesh refinement (AMR) hydrodynamical simulations that the efficiency for condensing out cool gas patches from non-linear perturbations depends critically on the ratio between the cooling time and the acceleration time (to reach the sound speed) in the gas. If cooling is efficient (such as in clumpy gas and/or in gas with a high-metallicity), cool patches can condense out in a Milky Way-type halo before being disrupted and may show up as 21 cm HVCs. The mixing of outflowing, metal-enriched fountain material and infalling coronal material possibly represents a key process that determines the net accretion through the disk-halo interface, as it regulates the cooling efficiency of the gas (Armillotta, Fraternali & Marinacci 2016; Marinacci et al. 2010).

Cosmologically “cold” ($T < T_{\text{vir}}$) streams of intergalactic gas are expected to feed the halos of Milky Way-type galaxies (e.g., van de Voort et al. 2011) and such streams may penetrate deep into the hot halo before they are being disrupted. From their AMR simulations, Fernandez, Joung & Putman (2012) find that cold streams from the IGM may continuously bring up to $\sim 10^8 M_{\odot}$ of H I into the Milky Way halo and this amount of neutral gas appears to be fairly constant over time (at least for the last 5 Gyr, or $z = 0 - 0.45$). The H I gas accretion rate for a Milky Way-type galaxy in these simulations comes out to $0.2 M_{\odot} \text{ yr}^{-1}$, thus very similar to what has been derived for the Galactic HVC population at $d < 20$ kpc, i.e., *without* the contribution of the MS (see Sect. 2.4).

Next to the cloud-condensation scheme and the cold streams, the interaction of Milky-Way type galaxies with dwarf satellites can transport large amounts of relatively cool gas in the halos of MW-type galaxies *directly*. From their study of a Milky-Way type galaxy and its satellite-galaxy environment Fernandez, Joung & Putman (2012) derive a median mass-loss rate of H I of $\sim 3 \times 10^{-3} M_{\odot} \text{ yr}^{-1}$, suggesting that satellites add $\sim 3 \times 10^6 M_{\odot}$ of neutral gas to the host galaxy within a Gyr. Based on their overall results, this H I mass flow represents a significant albeit not dominating contribution to the neutral gas accretion rate of the host galaxy. In the light of these results, the observed neutral gas supply from Magellanic Stream for the Milky Way ($M_{\text{HI,MS}} \sim 2.5 \times 10^8 M_{\odot}$ within 0.5 – 1.0 Gyr); see Sect. 2.1) is huge, underlining that the MS represents a rather extreme (and atypical) example for gas accretion by satellite interactions.

As suggested by Peek (2009), the specific angular momentum of the gas might be a key parameter to discriminate between the various scenarios for the origin of the HVCs. Gas that is accreted from dwarf satellites by either ram-pressure stripping or tidal interactions enters the halo with a large initial angular momentum ($L \sim 3 \times 10^4 \text{ km s}^{-1} \text{ kpc}$), while the angular momentum of the cooling halo clouds is one

order of magnitude less (see, e.g., Peek et al. 2008; Kaufmann et al. 2009). Thus, gas accretion from mergers with Milky Way satellites takes place predominantly in the outer regions ($R > 15$ kpc) of the Galactic disk. In fact, observations indicate that part of the MS (i.e., the Leading Arm) might already be close to the outer disk of the Milky Way, where it possibly already interacts with the underlying interstellar gas (McClure-Griffiths et al. 2008; Casetti-Dinescu et al. 2014), thus providing support for this scenario. Following Peek (2009), the HVCs at small galactocentric distances ($R < 15$ kpc), in contrast, are more likely to be produced by the condensed halo clouds and it is this process that appears to dominate the feeding of the inner-disk regions where most of the star formation takes place.

Independently of the origin of the infalling gas, how much of it makes it into the disk? To answer this crucial question for the Milky Way and other galaxies of similar mass and type, the initial conditions for the gas infall (e.g., infall velocities, individual cloud masses, density profile of the ambient coronal gas) turn out to be particularly important, as we will discuss in the following.

At $T = 10^6$ K in the coronal gas, the infall velocity of the HVCs is close to the sound speed in ambient hot medium ($v_s \sim 150 \text{ km s}^{-1}$), so that infalling material moves either in the subsonic, or transonic, or supersonic regime, leading to different ablation scenarios of infalling gas structures (Kwak et al. 2011). Using a grid-based hydrodynamical 3D code, Heitsch & Putman (2009) simulated the fate of H I clouds moving through the hot coronal gas to explore the characteristic morphologies of the infalling structures, such as head-tail structures, infall velocities, disruption path lengths, and timescales. In Fig. 6 we highlight some of their results. From their study it follows that H I clouds with relatively low initial masses of $M_{\text{cloud}} < 10^{4.5} M_{\odot}$ lose basically all their neutral gas content when infalling from $d = 10 - 12$ kpc. Thus, wherever such cloudlets might be formed in the halo, i.e., either from condensing out of the coronal gas or from dissolving infalling tidal or cosmological gas streams at much larger distances, their gas content will not reach the disk in *neutral* form. However, if the density contrast between the break-up material and the surrounding medium is large enough, the cloud remnants might reach the disk as warm ionized material (e.g., Shull et al. 2009; Heitsch & Putman 2009; Bland-Hawthorn 2009; Joung et al. 2012) or will otherwise fuel the Galactic Corona.

At the high-mass end, Kwak et al. (2011) predict that for cloud masses $M_{\text{cloud}} > 10^5 M_{\odot}$ up to 70 percent of the H I mass remains cool at $T < 10^4$, even after a possible break-up of the initial infalling cloud. Such massive structures may even survive the trip from larger distances, as they can move several hundred Myr through the hot halo before being destroyed completely. A similar conclusion was drawn from Joung, Bryan & Putman (2012) from their high-resolution AMR simulations (see above). This result is relevant for the Magellanic Stream at $d = 50 - 100$ kpc. Although observations suggest that the MS is further braking up into smaller gas clumps as it moves towards the Milky Way disk (e.g., Stanimirovic et al. 2002, 2008; Westmeier & Koribalski 2008; see also Tepper-Garcia et al. 2015), some dense cores with masses $M_{\text{cloud}} > 10^5 M_{\odot}$ may survive and these clumps could enter the disk in the form of neutral gas clouds.

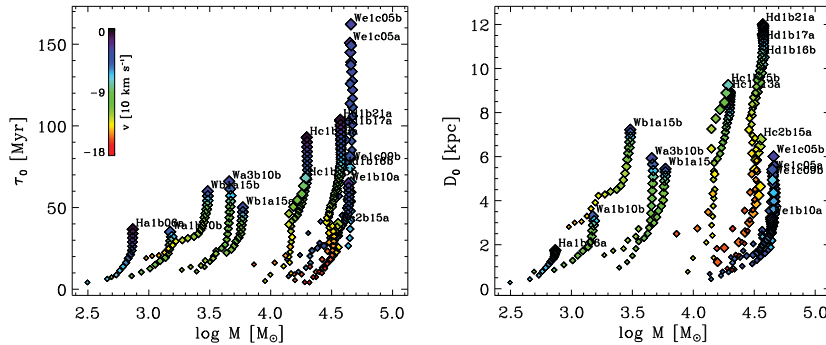


Fig. 6 Time sequences of cloud survival-times (left panel) and disruption length-scale (right panel) of neutral halo clouds of different mass that move through hot coronal gas in a Milky-Way type galaxy (Heitsch & Putman 2009). In these models, H I clouds with masses $< 10^{4.5} M_{\odot}$ do not survive their passage through the halo when infalling from $d = 10 - 12$ kpc. Figure adopted from Heitsch & Putman (2009).

Note that a certain fraction of the halo clouds that condense out of the coronal gas may also reach the disk *before* the gas cools efficiently, i.e., in the form of warm, ionized gas that never becomes neutral and visible in 21 cm emission. Those structures possibly explain some of the isolated high-velocity UV absorber that have no 21 cm counterparts (Collins, Shull & Giroux 2003; Collins et al. 2009; Shull et al. 2009; Richter et al. 2009; Fraternali et al. 2013; Marasco, Marinacci & Fraternali 2013; R17).

Even with the most advanced hydrodynamical simulations at hand, the exact role of many of the involved physical processes in the time evolution of accreted gas remains unclear. For instance, thermal conduction can suppress shear instabilities and thus stabilize clouds from evaporation by smoothing out steep density/temperature gradients between the cool infalling gas and the hot ambient medium (e.g., Vieser & Hensler 2007). However, such steep gradients appear to be unimportant for the cool/warm gas clouds in the Milky Way halo (e.g., Kwak et al. 2011) and also the diffusion by thermal conduction possibly is small compared to turbulent diffusion processes. Not all of the possibly relevant processes can be included simultaneously in the simulations. In particular, the role of magnetic fields (and resulting magneto-hydrodynamical effects) have been mostly ignored so far. Also, the spatial (or mass) resolution of many of the simulations discussed above still is very limited. Since early SPH simulation codes, for instance, had problems in resolving Kelvin-Helmholtz instabilities, cool circumgalactic gas clumps are artificially stabilized by SPH particle effects (Agertz et al. 2007), probably leading to misleading results.

In summary, hydrodynamical simulations predict that the life-time, the morphology, and the mass distribution of infalling gas clouds in the Milky Way halo depend strongly on the local boundary conditions under which the gas is generated and moving through the hot halo. Whether or not an infalling cool/warm gas cloud reaches the Milky Way disk in a region where it supplements star formation depends on

its initial distance to the disk, its mass and density, its infall velocity, its angular momentum, and other parameters.

3.2 Cosmological hydrodynamical simulations

Given the complexity of the physics of gas accretion outlined above and the strong dependence of the gas-accretion rate on the local boundary conditions, additional large-scale simulations are desired that also consider a realistic *cosmological* environment of the Milky Way. In particular, the role of a second nearby spiral galaxy (M31), the gas motions within the super-ordinate galaxy group environment (Local Group), as well as the streaming of intergalactic gas within the local cosmic web that connects the Local Group with its surrounding large-scale structure (e.g., the Virgo cluster) should be studied in such a context.

In a recent paper, N14 have studied the large-scale distribution and overall physical properties of gas in the Local Group and around Milky Way and M31 based on simulation data from the Constrained Local UniversE Simulations (CLUES) project (www.clues-project.org). In their study, the authors separate the circumgalactic and intragroup gas into three different phases: neutral gas, cold/warm ionized gas with $T < 10^5$ K, and hot gas with $T \geq 10^5$ K, similar as done here. The total neutral gas mass in the simulated Milky Way at galactocentric distances $d < 50$ kpc comes out to $M_{\text{HI}} \approx 3 \times 10^8 M_{\odot}$, thus in excellent agreement with the observations (Sect. 2.1). The total mass of the cold/warm ionized gas component is as large as $M_{\text{HII}} \approx 3 \times 10^{10} M_{\odot}$ for the entire halo out to the virial radius, but reduces to $M_{\text{HII}} \approx 2 \times 10^8 M_{\odot}$ for $d \leq 10$ kpc, where the bulk of UV absorption of warm-ionized gas is observed in the Milky Way (Lehner & Howk 2011; Sect. 2.2). The mass of the Milky Way's hot coronal gas in the simulation is $M_{\text{Corona}} \approx 4 \times 10^{10} M_{\odot}$ for $d \leq R_{\text{vir}}$ and $\approx 10^{10} M_{\odot}$ for $d \leq 100$ kpc, the latter value being consistent with the estimates from X-ray observations (Sect. 2.3). The Milky Way's neutral gas-accretion rate from gas at $d \leq 50$ kpc is estimated as $M_{\text{HI}} \approx 0.3 M_{\odot} \text{ yr}^{-1}$, which is only ~ 40 percent of the value derived from the 21 cm observations (Richter 2012), but more in line with what is expected for the neutral HVCs without the Magellanic Stream (Sect. 2.4). For larger distances to the disk, the neutral gas-accretion rate quickly falls below $10^{-2} M_{\odot} \text{ yr}^{-1}$ in the simulations (N14; their Fig. 14). The accretion rate of cold/warm gas instead is fairly independent of the distance for $d > 15$ kpc at a level of $M_{\text{HI}} \approx 5 M_{\odot} \text{ yr}^{-1}$, thus in line with the estimate from the UV observations (Fox et al. 2014; R17). Finally, the simulations imply that only for very large distances $d > 100$ kpc the accretion rate of hot ($T > 10^6$ K) gas dominates the mass inflow of gas for the Milky Way.

The influence of the Local Group environment in the simulations is reflected particularly in the anisotropic distribution of gas near the virial radius of the MW, because the gas follows the large-scale matter distribution in the elongated cosmological filament that forms the Local Group (N14). To visualize this, we show in Fig. 7 the gas distribution and gas kinematics around the simulated Milky Way and

M31 galaxies from the CLUES simulations. The two galaxies move towards the LG barycenter while the ambient gas is circulating around MW and M31 within the elongated filament in a complex pattern of infall and outflow channels. There is a significant gas excess between the two galaxies, as compared to any other direction, resulting from the overlap of their gaseous halos. Because of the Milky Way's flow towards LG barycenter, a velocity dipole pattern for high-ion absorption from LG gas/M31 halo gas is expected from a perspective within the Milky Way (R17). Such a dipole pattern is indeed observed in UV absorption in the direction of M31 and its antipode on the sky (Sect. 2.2). This possibly implies that warm/hot LG gas/M31 halo gas is pushed into the Milky Way halo due to the large-scale motion of both galaxies in their group environment. If true, this effect might cause a major boost in the Milky Way's future gas-accretion rate.

3.3 Comparison with observations

For a better understanding of the gas-accretion processes in the Milky Way, the comparison between observational data and predictions from simulations are essential. Next to the gas masses in the individual phases and the accretion rates (see above), the spatial distribution of the various gas phases in the simulations and their kinematics can be compared (in a statistical sense) with the observational constraints from 21 cm data and UV absorption spectra.

Combining 21 cm data from the Milky Way and M31, Richter (2012) predicted that the volume-filling factor of neutral gas in the halo of Milky-Way/M31 type galaxies declines exponentially with radius, leading to an exponential decline of the observed (projected) HI covering fraction. The study suggests that the covering fraction $f_c(\text{HI})$ drops below 0.05 for $d > 50$ kpc. A similar trend indeed has also been found in the recent CGM simulations of Milky-Way type galaxies (Fernandez, Joung & Putman 2012; N14), indicating that basically all neutral gas in MW-type galaxies is concentrated in the inner halo region. This conclusion is supported by the observed cosmological cross-section of neutral gas around low-redshift galaxies (Zwaan et al. 2005; Richter et al. 2011).

Also the apparent interaction between the MS and the surrounding coronal gas as well as the $\text{H}\alpha$ emission from the Stream have been investigated in simulations to reproduce the observational results. Bland-Hawthorn et al. (2007) and Tepper-Garcia et al. (2015) modeled the $\text{H}\alpha$ emission from the MS based on a shock-cascade model. Tepper-Garcia et al. (2015) conclude that the $\text{H}\alpha$ emission from the Stream can only be reproduced if the density of the ambient medium is $n_{\text{H}} = 2 - 4 \times 10^{-4} \text{ cm}^{-3}$, indicating that $\text{H}\alpha$ emitting regions in the MS must be within $d \leq 75$ kpc from the Galactic center.

Next to these examples, there are several other studies that have addressed these and other aspects by comparing observational results with simulations. Describing all of these unfortunately is beyond the scope of this review. Clearly, with future, more detailed simulations and additional constraints from multi-wavelength obser-

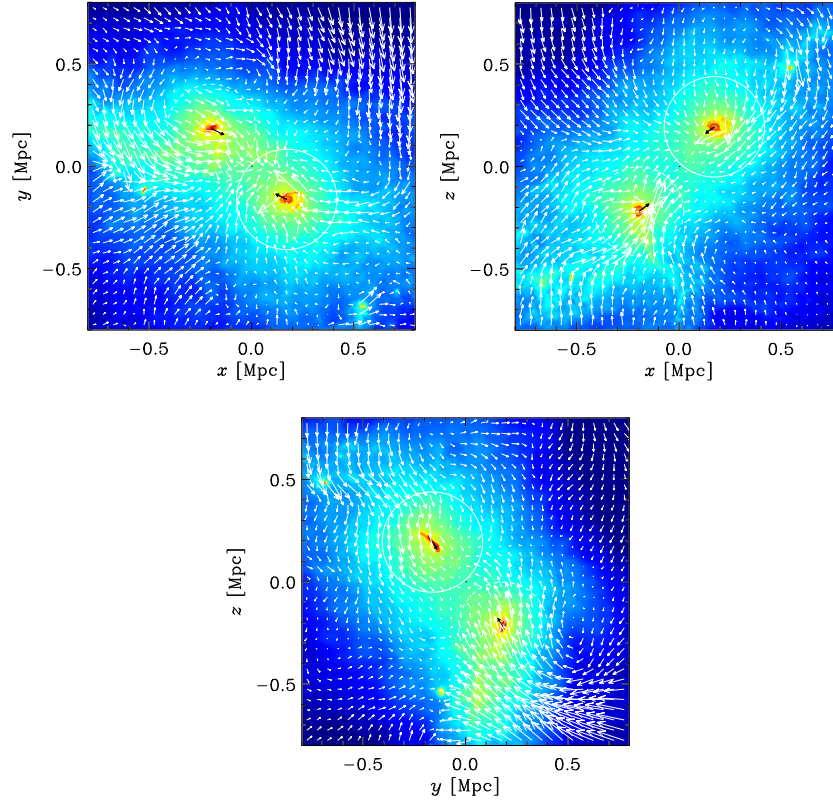


Fig. 7 Projected distribution and bulk motions of gas in and around the Milky Way (dashed circle, indicating the virial radius of the MW) and M31 (solid circle, indicating the virial radius of the M31) based on constrained cosmological simulations from the CLUES project (N14). Coordinates and velocities of the gas are given with respect to the Local Group barycenter in the x/y , x/z , and y/z planes, respectively. The white arrows show the velocity field of the gas, with the longest arrows representing a velocity of 130 km s^{-1} . The black arrows indicate the velocities of the MW and M31 galaxies. Their absolute space velocities are 67 and 76 km s^{-1} , respectively. Maps kindly provided by Sebastián Nuza.

vations the systematic combination of simulations and observations will provide crucial new insights into the properties of the Milky Way's CGM.

4 Concluding remarks

As for many other aspects of galaxy evolution, the Milky Way and its gaseous environment represent an excellent laboratory to study the details of gas-accretion processes of L^* galaxies in the local Universe. Although it remains a challenging

task to reconstruct the 3D distribution and galactocentric kinematics of the Milky Way's circumgalactic medium from an internal vantage point in the rotating disk, the combination of multi-wavelength observations of the gas in all its phases, the measurement and modeling of the stellar composition of the Milky Way disk and its star-formation rate and history, the numerical modeling of the hydrodynamic processes that shape the properties of the Galaxy's CGM, and the deep observations of the Milky Way and its satellite galaxies in a cosmological context together provide a particularly rich database that cannot be achieved for any other galaxy in the Universe.

The above discussed observations and simulations imply that the combination of gas infall, outflows, and mergers generates a multi-phase gaseous halo that is characterized by a highly complex spatial distribution of gas structures of different age and origin. The cycle of processes that is believed to lead to the continuous feeding of the Milky Way disk with fresh gas to supplement subsequent star-formation therein can be summarized as follows.

Cold and warm gas from the intergalactic medium and from satellite galaxies enters the Milky Way halo at its virial radius and is then processed by the ambient hot coronal gas. Fragments of the originally infalling gas may reach the disk in the form of warm or cold gas streams, while the remaining gas fraction is being incorporated into the hot Galactic Corona. In this way, the Corona is continuously fed with fresh gas from outside, while it is further stirred up and heated by gas outflowing from the star-forming disk and (eventually) from the Galactic center region (i.e., it is influenced by feedback processes). From the hot Corona, warm ionized and/or warm neutral gas patches may condense out through cooling processes, and these structures will sink down to the disk through the disk-halo interface, further contributing to the overall accretion rate of the Milky Way disk.

The accretion of cold and warm gas from the Magellanic Stream is a direct result of the interaction between the Milky Way and its population of satellite galaxies (here: the Magellanic Clouds). The MS adds more than 1 billion solar masses of gaseous material to the Milky Way halo, material that either directly or indirectly feeds the MW disk to supplement star formation therein. Thus, there is sufficient cold and warm gaseous material present in the outer halo to maintain the Milky Way's star-formation rate *in the far future* at its *current* level, although it remains unclear, how much of the material from the MS will finally end up in the disk (and at what time scale). The amount of gas that is currently being accreted through the disk-halo interface, and that will determine the star-formation rate *in the near future*, remains uncertain, however.

Our understanding of the gas-accretion processes in the Milky Way is far from being complete. On the observational side, additional constraints on distances and 3D velocities of the HVCs, the role of low-velocity halo gas, and the mass and spatial extent of the hot coronal gas based on multi-wavelength observations are highly desired on the long way towards a complete census of the Milky Way's circumgalactic gas. On the theoretical side, more advanced hydrodynamical simulations of the Milky Way's gaseous halo, that include all relevant physical processes in a realistic cosmological environment, will be of great importance to study the dynamics of gas

flows around the Galaxy. Finally, a systematic comparison between gas-accretion processes in the Milky Way and similar processes in other low- and high-redshift galaxies in the general context of galaxy evolution (with particular focus on environmental issues, feedback effects, and other important aspects) will provide crucial information that will help to better understand the cycling of gas on galactic and super-galactic scales. Many of these aspects will also be discussed in the following chapters.

Acknowledgements The author would like to thank Andy Fox, Matt Haffner, Fabian Heitsch, Jürgen Kerp, & Sebastián Nuza for providing helpful comments and supplementary material for the figures.

References

- Adams, W.S. 1949, *ApJ*, 109, 354
 Agertz, O., Moore, B., Stadel, J., et al. 2007, *MNRAS*, 380, 963
 Anderson, M.E., & Bregman, J.N. 2010, *ApJ*, 714, 320
 Armilotta, L., Fraternali, F., & Marinacci, F. 2016, *MNRAS*, 462, 4157
 Bajaja, E., Cappa de Nicolau, C.E., Cersosimo, J.C. et al. 1985, *ApJS*, 58, 143
 Bates, B., Catney, M.G., & Keenan, F.P. 1988, *ASS* 146, 195
 Bauermeister, A., Blitz, L., & Ma, C.-P. 2010, *ApJ*, 717, 323
 Begum, A., Stanimirovic, S., Peek, J.E.G., et al. 2010, *ApJ*, 722, 395
 Ben Bekhti, N., Richter, P., Westmeier, T., & Murphy, M.T. 2008, *A&A*, 487, 583
 Ben Bekhti, N., Winkel, B., Richter, P., et al. 2012, *A&A*, 542, A110
 Besla, G., Kallivayalil, N., Hernquist, L., et al. 2010, *ApJL*, 721, L97
 Besla, G., Kallivayalil, N., Hernquist, L., et al. 2012, *MNRAS*, 421, 210
 Birnboim, Y., & Dekel, A. 2003, *MNRAS*, 345, 349
 Blaauw, A. & Tolbert, C.R. 1966, *BAN*, 18, 405
 Bland-Hawthorn, J., Veilleux, S., Cecil, G. N., et al. 1998, *MNRAS*, 299, 611
 Bland-Hawthorn, J., & Putman, M. E. 2001, in *ASP Conf. Ser. 240, Gas and Galaxy Evolution*, ed. J. E. Hibbard, M. Rupen, J.H. van Gorkom, p. 369
 Bland-Hawthorn, J., & Maloney, P. R. 2002, in *ASP Conf. Ser. 254, Extragalactic Gas at Low Redshift*, ed. J. S. Mulchaey & J. T. Stocke (San Francisco, CA: PASP), p. 267
 Bland-Hawthorn, J., & Cohen, M. 2003, *ApJ*, 582, 246
 Bland-Hawthorn, J., Sutherland, R., Agertz, O., & Moore, B. 2007, *ApJL*, 670, L109
 Bland-Hawthorn, J. 2009, *IAUS*, 254, 241
 Bland-Hawthorn, J., Maloney, P., Sutherland, R.S., & Madsen, G.J. 2013, *ApJ*, 778, 58
 Blitz, L., Spiegel, D.N., Teuben, P.J., Hartmann, D., & Burton, W.B. 1999, *ApJ*, 514, 818
 Bregman, J.N. & Lloyd-Davies, E.J. 2007, *ApJ*, 669, 990
 Bregman, J.N. 2007, *ARA&A*, 45, 221
 Braun, R. & Burton, W.B. 1999, *A&A*, 341, 437
 Brooks, A.M., Governato, F., Quinn, T., Brook, C.B., & Wadsley, J. 2009, *ApJ*, 694, 396
 Brüns, C., Kerp, J., Staveley Smith, L., et al. 2005, *A&A*, 432, 45
 Burkert, A., & Lin, D.N.C. 2000, *ApJ*, 537, 270
 Casetti-Dinescu, D.I., Moni Bidin, C., Girard, T.M., et al. 2014, *ApJL*, 784, L37
 Chiappini, C., Matteucci, F., & Romano, D. 2001, *ApJ*, 554, 1044
 Chomiuk, L. & Povich, M.S. 2011, *AJ*, 142, 197
 Collins, J.A., Shull, J.M., & Giroux, M.L. 2003, *ApJ*, 585, 336
 Collins, J.A., Shull, J.M., & Giroux, M.L. 2005, *ApJ*, 623, 196

- Collins, J.A., Shull, J.M., & Giroux, M.L. 2009, ApJ, 705, 962
- Connors, T.W., Kawata, D., & Gibson, B.K. 2006, MNRAS, 371, 108
- de Heij, V., Braun, R. & Burton, W.B. 2002, A&A, 391, 67
- Desert, F.-X., Bazell, D. & Boulanger, F. 1988, ApJ, 334, 815
- Desert, F.-X., Bazell, D. & Blitz, L. 1990, ApJ, 355, L51
- Dettmar, R.-J. 1990, A&A, 232, L15
- Diaz, J.D., & Bekki, K. 2011, ApJ, 413, 2015
- Diaz, J.D., & Bekki, K. 2012, ApJ, 750, 36
- Dieter, N.H. 1964, AJ, 79, 288
- Di Teodoro, E.M. & Fraternali, F. 2014, A&A, 567, 68
- D'Onghia, E. & Fox, A.J. 2016, ARA&A, 54, 363
- Elson, E.C., de Blok, W.J.G. & Kraan-Korteweg, R.C. 2011, MNRAS, 411, 200
- Fang, T., Marshall, H.L., Lee, J.C., Davis, D.S., & Canizares, C.R. 2002, ApJ, 572, L127
- Fang, T., Sembach, K.R., & Canizares, C.R. 2003, ApJ, 586, L49
- Fang, T., McKee C.F., Canizares, C.R., & Wolfire, M. 2006, ApJ, 644, 174
- Fang, T., Bullock, J. & Boylan-Kolchin, M. 2013, ApJ, 762, 20
- Fernandez, X., Joung, M. R., & Putman, M. E. 2012, ApJ, 749, 181
- Ferriere, K. 2001, RvMP, 73, 103
- Ford, H.A., Lockman, F.J. & McClure-Griffiths, N.M. 2010, 722, 367
- Fox, A.J., Savage, B.D., Wakker, B.P., et al. 2004, ApJ, 602, 738
- Fox, A.J., Wakker, B.P., Savage, B.D., et al. 2005, ApJ, 630, 332
- Fox, A.J., Wakker, B.P., Smoker, J.V., et al. 2010, ApJ, 718, 1046
- Fox, A.J., Richter, P., Wakker, B.P., et al. 2013, ApJ, 772, 110
- Fox, A.J., Wakker, B.P., Barger, A., et al. 2014, ApJ, 787, 147
- Fox, A.J., Bordoloi, R., Savage, B.D., et al. 2015, ApJ, 799, L7
- Fox, A.J., Lehner, N., Lockman, F.J. et al. 2016, ApJ, 816, L11
- Fraternali, F. & Binney, J.J. 2008, MNRAS, 386, 935
- Fraternali, F., Marasco, A., Marinacci, F., & Binney, J.J. 2013, ApJL, 764, L21
- Fumagalli, M., Prochaska, J.X., Kasen, D., et al. 2011, MNRAS, 418, 1796
- Gardiner, L.T. & Noguchi, M. 1996, MNRAS, 278, 191
- Gaensler, B.M., Madsen, G.J., Chatterjee, S. & Mao, S.A. 2008, PASA, 25, 184
- Gibson, B.K., Giroux, M.L., Penton, S.V., et al. 2001, AJ, 122, 3280
- Gillmon, K., Shull, J.M., Tumlinson, J., & Danforth, C. 2006, ApJ, 636, 891
- Grcevich, J., & Putman, M. E. 2009, ApJ, 696, 385
- Gupta, A., Mathur, S., Krongold, Y., Nicastro, F., & Galeazzi, M. 2012, ApJ, 756, L8
- Haffner, L.M., Reynolds, R.J., Tufte, S.L., et al. 2003, ApJS, 149, 405
- Haffner, L.M., Reynolds, R.J., Babler, B.L., et al. 2016, Proc. AAS, 227, id347
- Hartmann, D., & Burton, W. B. 1997, *Atlas of Galactic Neutral Hydrogen*, (Cambridge: Cambridge Univ. Press)
- Herenz, P., Richter, P., Charlton, J.C., & Masiero, J.R. 2013, A&A, 550, A87
- Heitsch, F., & Putman, M. E. 2009, ApJ, 698, 1485
- Hernandez, A.K., Wakker, B.P., Benjamin, R.A., et al. 2013, ApJ, 777, 19
- Hill, A.S., Haffner, L.M., & Reynolds, R.J. 2009, ApJ, 703, 1832
- Houck, J.C. & Bregman, J.N. 1990, ApJ, 352, 506
- Hulsbosch, A.N.M. & Wakker, B.P. 1988, A&AS, 75, 191
- Hulsbosch, A.N.M. & Raimond, R. 1966, BAN, 18, 413
- Jin, S. & Lynden-Bell, D. 2008, MNRAS, 383, 1686
- Joung, M.R., Bryan, G.L., & Putman, M.E. 2012, ApJ, 745, 148
- Joung, M.R., Putman, M.E., Bryan, G.L., Fernandez, X., & Peek, J.E.G. 2012, ApJ, 759, 137
- Kalberla, P.M.W., Burton, W.B., Hartmann, D., et al. 2005, A&A, 440, 775
- Kalberla, P.M.W. & Kerp, J. 2009, ARA&A, 47, 27
- Kaufmann, T., Mayer, L., Wadsley, J., Stadel, J., & Moore, B. 2006, MNRAS, 370, 1612
- Kaufmann, T., Bullock, J.S., Maller, A.H., Fang, T., & Wadsley, J. 2009, MNRAS, 396, 191
- Kereš, D., Katz, N., Weinberg, D.H., & Dave, R. 2005, MNRAS, 363, 2

- Kereš, D. & Hernquist, L. 2009, ApJL, 700, L1
- Kerp, J., Burton, W.B., Egger, R., et al. 1999, A&A, 342,213
- Kuntz, K.D. & Danly, L. 1996, ApJ, 457, 703
- Kuntz, K.D. & Snowden, S.L. 2000, ApJ, 543, 195
- Kwak, K., Henley, D.B. & Shelton, R.L. 2011, ApJ, 739,30
- Larson, R.B. 1972, Nature, 236,21
- Lehner N. 2002, ApJ, 578,126
- Lehner, N., & Howk, J.C. 2011, Sci, 334, 955
- Lehner, N., Howk, J.C., Thom, C., et al. 2012, MNRAS, 424, 2896
- Levine, E.S., Blitz, L. & Heiles, C. 2006, ApJ, 643, 881
- Lockman, F.J. 2002, ApJL, 580, L47
- Lockman, F.J., Murphy, E.M., Petty-Powell, S., & Urlick, V.J. 2002, ApJS, 140, 331
- Lockman, F.J., Benjamin, R.A., Heroux, A.J., & Langston, G.I. 2008, ApJL, 679, L21
- MacLow, M. & Klessen, R. 2004, RvMP, 76, 125
- Maller, A.H. & Bullock, J.S. 2004, MNRAS, 355,694
- Marasco, A., Marinacci, F., & Fraternali, F. 2013, MNRAS, 433, 1634
- Marinacci, F., Binney, J.J., Fraternali, F., et al. 2010, MNRAS, 404, 1464
- Mathewson, D.S. 1967, PASA, 1, 21
- Mathewson, D.S., Cleary, M.N., & Murray, J.D. 1974, ApJ, 190, 291
- Mathur, S., Weinberg, D. H., & Chen, X. 2003, ApJ, 582, 82
- McClure-Griffiths, N.M., Staveley-Smith, L., Lockman, F.J., et al. 2008, ApJL, 673, L143
- McClure-Griffiths, N.M., Pisano, D.J., Calabretta, M.R., et al. 2009, ApJS, 181, 398
- McKernan, B., Yaqoob, T., & Reynolds, C.S. 2004, ApJ, 617, 232
- Miller, M.J., & Bregman, J.N. 2013, ApJ, 770, 118
- Miller, M.J., & Bregman, J.N. 2015, ApJ, 800, 14
- Miller, M.J., Kluck, E.J. & Bregman, J.N. 2016, ApJ, 818, 112
- Miville-Deschênes, M.A., Boulanger, F., Reach, W.T. & Noriega-Crespo, A. 2005, ApJ, 631, L57
- Mo, H.J., Miralda-Escude, J. 1996, ApJ, 469, 589
- Morras, R., Bajaja, E., Arnal, E.M. & Pöppel, W.G.L. 2000, A&AS, 142, 25
- Morton, D.C. 2003, ApJS, 149, 205
- Muller, C.A., Oort, J.H., & Raimond, E. 1963, C.R. Acad. Sci. Paris, 257, 1661
- Münch, G. 1952, PASP, 64, 312
- Münch, G. & Zirin, H. 1961, ApJ, 133, 11
- Murphy, E.M., Lockman, F.J., & Savage, B.D. 1995, ApJ, 447, 642
- Murray, C.E., Stanimirovic, S., McClure-Griffiths, N.M. et al. 2015, ApJ, 808, 41
- Nichols, M. & Bland-Hawthorn, J. 2011, ApJ, 732, 17
- Nidever, D.L., Majewski, S.R., Butler Burton, W., & Nigra, L. 2010, ApJ, 723, 1618
- Nuza, S.E., Parisi, F., & Scannapieco, C., et al. 2014, MNRAS, 441, 2593
- Oort, J.H. 1966, BAN, 18, 421
- Peebles, P.J.E., Phelps, S.D., Shaya, E.J., & Tully, R.B. 2001, ApJ, 554, 104
- Peebles, P.J.E., Tully, R.B., & Shaya, E.J. 2011, preprint (arXiv:1105.5596)
- Peek, J.E.G., Putman, M.E., McKee, C.F., Heiles, C., & Stanimirovic, S. 2007, ApJ, 656,907
- Peek, J.E.G., Putman, M.E., & Sommer-Larsen, J. 2008, ApJ, 674,227
- Peek, J.E.G. 2009, ApJ, 698, 1429
- Peek, J.E.G., Heiles, C., Putman, M.E., & Douglas, K. 2009, ApJ, 692, 827
- Planck Collab.: Abergel, A., Ade, P.A.R., Aghanim, N. et al. 2011, A&A, 536, A24
- Prata, S., & Wallerstein, G. 1967, PASP, 79, 202
- Putman, M.E., Gibson, B.K., Staveley-Smith, L., et al. 1998, Nature, 394, 752
- Putman, M.E., Staveley-Smith, L., Freeman, K.C., Gibson, B.K., & Barnes, D.G. 2003, ApJ, 586, 170
- Putman, M.E., Peek, J.E.G., & Joung, M.R. 2012, ARA&A, 50, 491
- Rasmussen, A., Kahn, S. M., & Paerels, F. 2003, in ASSL Conf. Proc. 281, *The IGM/Galaxy Connection. The Distribution of Baryons at $z = 0$* , ed. J.L. Rosenberg & M.E. Putman (Dordrecht: Kluwer), 109

- Rana, N. 1991, *ARA&A*, 29, 129
- Rees, M.J. & Ostriker, J.P. 1977, *MNRAS*, 179, 541
- Reynolds, R.J. 1991, *ApJ*, 372, L17
- Reynolds, R.J., Haffner, L.M., Madsen, G.J., Wood, K., & Hill, A.S. 2012, *EAS*, 56, 213
- Richter, P., de Boer, K.S., Bomans, D.J., et al. 1999, *Nature*, 402, 386
- Richter, P., Sembach, K.R., Wakker, B.P., & Savage, B.D. 2001a, *ApJ*, 562, L181
- Richter, P., Savage, B.D., Wakker, B.P., Sembach, K.R., Kalberla, P.M.W. 2001b, *ApJ*, 549, 281
- Richter, P., Sembach, K.R., & Howk, J.C. 2003a, *A&A*, 405, 1013
- Richter, P., Wakker, B.P., Savage, B.D., & Sembach, K.R. 2003b, *ApJ*, 586, 230
- Richter, P. 2006, *RvMA* 19, 31
- Richter, P., Paelers, F.B.S., & Kaastra, J.S. 2008, *SSRv*, 134, 25
- Richter, P., Charlton, J.C., Fangano, A.P.M., Ben Bekhti, N., & Masiero, J.R. 2009, *ApJ*, 695, 1631
- Richter, P., Krause, F., Fechner, C., Charlton, J.C., & Murphy, M.T. 2011, *A&A*, 528, A12
- Richter, P. 2012, *ApJ*, 750, 165
- Richter, P., Fox, A. J., Wakker, B. P., et al. 2013, *ApJ*, 772, 111
- Richter, P., de Boer, K.S., Werner, K., & Rauch, T. 2015, *A&A*, 584, L6
- Richter, P., Wakker, B.P., Fechner, C., et al. 2016, *A&A*, 590, A68
- Richter, P., Ben Bekhti, N., Nuza, S.E., et al. 2017, *A&A*, submitted (R17)
- Robitaille, T.P., & Whitney, B.A. 2010, *ApJL*, 710, L11
- Röhser, T., Kerp, J., Lenz, D., & Winkel, B. 2016, *A&A*, in press (arXiv:1609.06540)
- Salem, M., Besla, G., Bryan, G., et al. 2015, *ApJ*, 815, 77
- Saul, D.R., Peek, J.E.G., Grcevich, J., et al. 2012, *ApJ*, 758, 44
- Savage, B.D. & Sembach, K.R. 1996, *ARA&A*, 34, 279
- Savage, B.D., Sembach, K.R., Wakker, B.P., et al. 2003, *ApJS*, 146, 125
- Savage, B.D. & Wakker, B.P. 2009, *ApJ*, 702, 1472
- Sellwood, J.A. & Binney, J.J. 2002, *MNRAS*, 336, 785
- Sembach, K.R., Howk, J.C., Savage, B.D., & Shull, J.M. 2001, *AJ*, 121, 992
- Sembach, K.R., Wakker, B.P., Savage, B.D., Richter, P. et al. 2003, *ApJS*, 146, 165
- Sembach, K.R., Wakker, B.P., Tripp, T.M. 2004, *ApJS*, 150, 387
- Shapiro, P.R. & Field, G.B. 1976, *ApJ*, 205, 762
- Shen, S., Madau, P., Guedes, J., et al. 2013, *ApJ*, 765, 89
- Shull, J.M., Jones, J.R., Danforth, C.W., & Collins, J.A. 2009, 699, 754
- Smith, G.P. 1963, *BAN*, 17, 203
- Smoker, J.V., Fox, A.J., & Keenan, F.P. 2011, *MNRAS*, 415, 1105
- Sommer-Larsen, J. 2006, *ApJL*, 644, L1
- Spitzer, L. 1956, *ApJ*, 124, 40
- Springel, V. & Hernquist, L. 2005, *ApJ*, 622, L9
- Stanimirović, S., Dickey, J.M., Krco, M., & Brooks, A.M. 2002, *ApJ*, 576, 773
- Stanimirović, S., Hoffman, S., Heiles, C., et al. 2008, *ApJ*, 680, 276
- Su, M., Slatyer, T.R., & Finkbeiner, D.P. 2010, *ApJ*, 724, 1044
- Tepper-Garcia, T., Bland-Hawthorn, J., & Sutherland, R.S. 2015, *ApJ*, 813, 94
- Thom, C., Putman, M. E., Gibson, B. K., et al. 2006, *ApJ*, 638, L97
- Thom, C., Peek, J. E. G., Putman, M. E., et al. 2008, *ApJ*, 684, 364
- Tripp, T.M., Wakker, B.P., Jenkins, E.B., et al. 2003, *AJ*, 125, 3122
- Tripp, T. M., & Song, L. 2012, *ApJ*, 746, 173
- Tufte, S.L., Reynolds, R.J., & Haffner, L.M. 1998, *ApJ*, 504, 773
- Tufte, S.L., Wilson, J.D., Madsen, G.J., Haffner, L.M., & Reynolds, R.J. 2002, *ApJL*, 572, L153
- van den Bergh, S. 1962, *AJ*, 67, 486
- van de Voort, F., Schaye, J., Booth, C.M., Haas, M.R., & Dalla Vecchia, C. 2011, *MNRAS*, 414, 2458
- van de Voort, F., & Schaye, J. 2012, *MNRAS*, 423, 2991
- van Woerden, H., Schwarz, U.J., Peletier, R.F., Wakker, B.P., & Kalberla, P.M.W. 1999, *Nature*, 400, 138

- van Woerden, H., Wakker, B.P., Schwarz, U.J., & de Boer, K.S. 2004, *High Velocity Clouds*, (Dordrecht: Kluwer)
- Vieser, W. & Hensler, G. 2007, *A&A*, 475, 251
- Vogelsberger, M., Sijacki, D., Keres, D., Springel, V., & Hernquist, L. 2012, *MNRAS*, 425, 3024
- Wakker, B.P., & Boulanger, F. 1986, *A&A*, 170, 84
- Wakker, B.P. & van Woerden, H. 1991, *A&A*, 250, 509
- Wakker, B.P. & van Woerden, H. 1998, *ARA&A*, 35, 217
- Wakker, B.P., Howk, J.C., Savage, B.D. 1999, *Nature*, 402, 388
- Wakker, B.P. 2001, *ApJS*, 136, 463
- Wakker, B.P., Savage, B.D., Sembach, K.R., et al. 2003, *ApJS*, 146, 1
- Wakker, B.P. 2004, in *High Velocity Clouds*, ed. H. van Woerden, B.P. Wakker, U.J. Schwarz, & K.S. de Boer (Dordrecht: Kluwer), 25
- Wakker, B.P. 2006, *ApJS*, 163, 282
- Wakker, B.P., York, D.G., Howk, J.C., et al. 2007, *ApJ*, 670, L113
- Wakker, B.P., York, D.G., Wilhelm, R., et al. 2008, *ApJ*, 672, 298
- Wang Q.D., Yao, Y., Tripp, T.M., et al. 2005, *ApJ*, 635, 386
- Weiner, B., & Williams, T. 1996, *AJ*, 111, 1156
- Weiss, A., Heithausen, A., Herbstmeier, U., & Mebold, U. 1999, *A&A*, 344, 955
- Westmeier, T., Braun, R., Brüns, C., Kerp, J., & Thilker, D.A. 2007, *New. Astron. Rev.*, 51, 108
- Westmeier, T. & Koribalski, B.S. 2008, *MNRAS*, 388, L29
- White, S.D.M. & Frenk, C.S. 1991, *ApJ*, 379, 52
- White, S.D.M. & Rees, M.J. 1978, *MNRAS*, 183, 341
- Whiting, A.B. 2014, *ApJ*, 793, 63
- Williams, R.J., Mathur, S., Nicastro, F., et al. 2005, *ApJ*, 631, 856
- Williams, R.J., Mathur, S., Poindexter, S., Elvis, M., & Nicastro, F., 2012, *AJ*, 143, 82
- Winkel, B., Kalberla, P.M.W., Kerp, J., Flöer, L. 2010, *ApJS*, 188, 488
- Winkel, B., Ben Bekhti, N., Darmstädter, V., et al. 2011, *A&A*, 533, A105
- Yao, Y., Nowak, M.A., Wang, Q.D., Schulz, N.S., & Canizares, C.R. 2008, *ApJ*, 672, L21
- Zech, W., Lehner, N., Howk, J.C., Dixon, W., & Brown, T. 2008, *ApJ*, 679, 460
- Zheng, Y., Putman, M.E., Peek, J.E.G., & Joungh, M.R. 2015, *ApJ*, 807, 103
- Zwaan, M., van der Hulst, J.M., Briggs, F.H., Verheijen, M.A., & Ryan-Weber, E.V. 2005, *MNRAS*, 364, 1467